

1 Composition and Vertical Flux of Particulate Organic Matter to the Oxygen Minimum Zone
2 of the Central Baltic Sea: Impact of a sporadic North Sea Inflow

3

4

5 Carolina Cisternas-Novoa^{1*}, Frédéric A.C. Le Moigne^{1,2}, Anja Engel¹.

6 ¹ *GEOMAR, Helmholtz Centre for Ocean Research Kiel, Düsternbrooker Weg 20, D-24105*
7 *Kiel*

8 ² *Present address: "Mediterranean Institute of Oceanography, UM 110, Aix Marseille Univ.,*
9 *Université 6 de Toulon, CNRS, IRD, 13288, Marseille, France"*

10 **Corresponding author: Carolina Cisternas-Novoa, GEOMAR, Helmholtz Centre for Ocean*
11 *Research Kiel, Düsternbrooker Weg 20, D-24105 Kiel, Germany, +49 431 600-4146*
12 *ccisternas@geomar.de*

13 *Keywords: Baltic Sea, Oxygen minimum zone, POC, PN, POP, TEP, CSP, Sediment trap,*
14 *Export efficiency.*

15

Abstract

Particle sinking is a major form to transport photosynthetically fixed carbon below the euphotic zone via the biological carbon pump (BCP). Oxygen (O₂) depletion may improve the efficiency of the BCP. However, the mechanisms by which O₂-deficiency can enhance particulate organic matter (POM) vertical fluxes are not well understood. Here, we investigate the composition and vertical fluxes of POM in two deep basins of the Baltic Sea (GB: Gotland basin and LD: Landsort Deep). The two basins showed different oxygen regimes resulting from the intrusion of oxygen-rich water from the North Sea that ventilated the water column below 140 m in GB, but not in LD. In June 2015, we deployed surface-tethered drifting sediment traps in oxic surface waters (GB: 40 and 60 m; LD: 40 and 55m), within the oxygen minimum zone (OMZ, GB: 110 m and LD: 110 and 180 m), and at recently oxygenated waters by the North Sea inflow in GB (180 m). The primary objective of this study was to test the hypothesis that the different O₂ conditions in the water column of GB and LD affected the composition and vertical flux of sinking particles, and caused differences in export efficiency between those two basins.

Composition and vertical flux of sinking particles were different in GB and LD. In GB, particulate organic carbon (POC) flux was 18% lower in the shallowest trap (40 m) than in the deepest sediment trap (at 180 m). Particulate nitrogen (PN) and Coomassie stainable particles (CSP) fluxes decreased with depth, while particulate organic phosphorus (POP), biogenic silicate (BSi), chlorophyll *a* (Chl *a*), and transparent exopolymeric particles (TEP) fluxes peaked within the core of the OMZ (110 m); this coincided with the presence of manganese oxide (MnOx)-like particles aggregated with organic matter. In LD, vertical fluxes of POC, PN, and CSP decreased by 28, 42 and 56% respectively, from the surface to deep waters. POP, BSi and TEP fluxes did not decrease continuously with depth, but they were higher at 110 m. Although we observe higher vertical flux of POP, BSi and TEP coinciding with abundant MnOx-like particles at 110 m in both basins, the peak in the vertical flux of POM and MnOx-like particles was much higher in GB than in LD. Sinking particles were remarkably enriched in BSi, indicating that diatoms were preferentially included in sinking aggregates and/or there was an inclusion of lithogenic Si

44 (scavenged into sinking particles) in our analysis. During this study, the POC transfer efficiency
45 (POC flux at 180 m over 40 m) was higher in GB (115%) than in LD (69%) suggesting that under
46 anoxic conditions a smaller portion of the POC exported below the euphotic zone was transferred
47 to 180 m than under re-oxygenated conditions present in GB. In addition, the vertical fluxes of
48 MnOx-like particles were two orders of magnitude higher in GB than at LD. Our results suggest
49 that POM aggregate with MnOx-like particles formed after the inflow of oxygen-rich water into
50 GB, the formation of those MnOx-OM rich particles may alter the composition and vertical flux
51 of POM, potentially contributing to a higher transfer efficiency of POC in GB. This idea is
52 consistent with observations of fresher and less degraded organic matter in deep waters of GB
53 than LD.

54 **1. Introduction**

55 Particle sinking is the primary mechanism for transporting photosynthetically fixed carbon below
56 the euphotic zone via the biological carbon pump (BCP) (Boyd and Trull, 2007; Turner, 2015).
57 Previous studies suggested that the transfer of particulate organic carbon (POC) from the euphotic
58 zone to the ocean interior is enhanced in oxygen minimum zones (OMZs) (Cavan et al., 2017;
59 Devol and Hartnett, 2001; Engel et al., 2017; Keil et al., 2016; Van Mooy et al., 2002). Possible
60 mechanisms explaining the higher POC transfer include: i) the reduction of aggregate
61 fragmentation due to the lower zooplankton abundance within the OMZ (Cavan et al., 2017; Keil
62 et al., 2016); ii) the potentially high contribution of refractory terrestrial organic matter (OM) to
63 the POC flux (Keil et al., 2016; Van Mooy et al., 2002); iii) a decrease in heterotrophic microbial
64 activity due to oxygen (O₂) limitation (Devol and Hartnett, 2001); iv) the preferential degradation
65 of nitrogen-rich organic compounds (Kalvelage et al. 2013; Van Mooy et al. 2002, Engel et al.
66 2017), and v) changes in ballast materials that may alter the sinking velocity and protect OM from
67 degradation (Armstrong et al., 2002). Currently, the study of POC vertical flux in OMZ's has
68 been mostly focused on the tropical ocean (Cavan et al., 2017; Devol and Hartnett, 2001; Engel et
69 al., 2017; Keil et al., 2016; Van Mooy et al., 2002); whereas, how low O₂ concentration would

70 affect the composition and fate of sinking OM, and the efficiency of the BPC in oxygen-deficient
71 zones of temperate-boreal regimes such as the Baltic deep basins had been less studied.

72 The semi-enclosed, brackish Baltic Sea is a unique environment with strong natural gradients of
73 salinity and temperature (Kullenberg and Jacobsen, 1981), primary productivity, nutrients
74 (Andersen et al., 2017), and O₂ concentrations (Carstensen et al., 2014a). New production,
75 defined as the fraction of the autotrophic production supported by allochthonous sources of
76 nitrogen (Dugdale and Goering, 1967) is considered equivalent to the particulate OM export
77 (Eppley and Peterson, 1979; Legendre and Gosselin, 1989) on appropriate timescales. In the
78 Baltic Sea, new production varies seasonally (Thomas and Schneider, 1999); with periods of high
79 new production during spring and summer, supported by the diatom-dominated spring bloom and
80 by diazotrophic cyanobacteria respectively (Wasmund and Uhlig, 2003). Based on sediment trap
81 data, collected at 140 m depth in the Gotland Basin (GB), Struck et al. (2004) reported that the
82 highest fluxes of POC occurred in fall, followed by summer and spring. Using $\delta^{15}\text{N}$, they showed
83 that during the summer, N₂ fixation by diazotrophic species is the primary source (~41%) of the
84 exported nitrogen and that the majority of the sedimentary particulate organic matter (POM) in
85 the central Baltic Sea is of pelagic origin.

86 OM export from the euphotic zone to the seafloor has a dual significance in the deep basins of the
87 Baltic Sea. On the one hand, it contributes to the long-term burial of POC, and consequently to
88 the removal and long-term storage of CO₂ from surface waters (Emeis et al., 2000; Leipe et al.,
89 2011), and on the other hand, it connects the pelagic and the benthic systems contributing to the
90 O₂ consumption and hence deoxygenation at depth. Environmental and anthropogenic changes
91 may alter the magnitude and composition of OM transferred from the surface to the seafloor in the
92 Baltic Sea (Tamelander et al. 2017). The reduction of nutrient inputs as targeted by the Baltic
93 Marine Environment Protection Commission (HELCOM) may reduce in OM downward flux and
94 limit the oxygen depletion at depth. However, since hypoxia occurred naturally in the Baltic Sea
95 due to physical processes, mitigating eutrophication will only decrease the spatial extent and
96 intensity of the O₂ deficiency in the deep basins.

97 GB (248 m) and Landsort Deep (LD, 460 m) are the deepest basins of the Baltic Sea. They exhibit
98 permanent bottom-water hypoxia (Conley et al. 2002), caused by a combination of limited water
99 exchange with the North Sea through the Kattegat, strong vertical stratification, and high
100 production /rem mineralization of OM due to eutrophication (Carstensen et al., 2014b; Conley et al.,
101 2009). A permanent transition zone of about 2 to 10 m thickness separates the oxygenated surface
102 and the oxygen-deficient waters, with a pelagic redoxcline located approximately between 127
103 and 129 m in GB, and between 79 and 85 m in LD (Glockzin et al., 2014). From the 1950s to
104 1970s, the hypoxic zones ($<60 \mu\text{M}$) in the Baltic Sea had expanded fourfold (Carstensen et al.
105 2014). Salt-water inflows from the North Sea are the primary mechanism renewing deep water in
106 the central Baltic Sea (Günter et al., 2008). A Major Baltic Inflow (MBI) occurred in 2014/2015
107 (Mohrholz et al. 2015); this event ventilated bottom waters for five months between February and
108 July 2015 (Holtermann et al., 2017). This MBI caused the intrusion of O_2 to deep hypoxic waters,
109 substantial temperature variability (Holtermann et al., 2017), displacement of remnant stagnant
110 water masses by new water that changed the chemistry of the water column (Myllykangas et al.,
111 2017), and high turbidities that may be associated with redox reactions products (Schmale et al.,
112 2016). At the time of sampling (June 2015), the MBI had reached GB but did not affect LD,
113 located further northwest. The oxygenated water inflow reached GB at the beginning of March
114 and created a secondary near-bottom redoxcline (Schmale et al., 2016); the bottom water anoxia
115 started to re-established in July 2015 (Dellwig et al., 2018). In LD, water properties did not
116 change due to the MBI, the sulfidic layer was maintained (hydrogen sulfide, H_2S concentrations
117 of $20.7\text{-}21.2 \mu\text{M}$), and salinity varied between 10.6 and 10.9 (Holtermann et al., 2017).

118 Pelagic redoxclines are the suboxic transition between oxic and anoxic - even sulfidic- waters. A
119 steep redox gradient characterizes this transition zone where electron acceptors and their reduced
120 counterparts are vertically segregated, and biogeochemical transformations mediated by microbial
121 processes are actively occurring (Bonaglia et al., 2016; Brettar and Rheinheimer, 1991; Neretin et
122 al., 2003). For instance, iron (Fe) and manganese (Mn) undergo rapidly reversible transformations
123 at the redox interface. Mn is an essential electron donor and acceptor in redox processes occurring

124 at brackish, pelagic systems with anoxic conditions like the deep basins of the Baltic Sea. Redox
125 conditions control the biogeochemical transformations between dissolved Mn^{2+} and insoluble
126 oxides and hydroxides of Mn^{4+} . Under anoxic conditions dissolved reduced Mn forms dominates,
127 while in the presence of O_2 the formation of particulate manganese oxides (MnOx) is favored.
128 The concentration of dissolved Mn may reach 0.3 μM in GB and a maximum value of about 3
129 μM in the LD (Dellwig et al., 2012). van Hulst et al. (2017) estimated an aggregation threshold
130 for manganese oxides of 25 pM, and suggested that a minimal concentration of dissolved Mn is
131 required for an efficient aggregation and removal of MnOx. Therefore, in GB and LD, the balance
132 between dissolved Mn and the formation of MnOx is controlled by the O_2 availability (e.g., Neretin
133 et al., 2003). LD is characterized by a permanently stratified water column and sulfidic bottom
134 waters; these conditions favored the accumulation of high concentrations of dissolved Mn
135 (Dellwig et al., 2012).

136 In contrast, GB is periodically affected by lateral intrusions of O_2 and the oxygenation of deep
137 water as a result of MBI that occur every one to four years (Matthäus and Franck, 1992), favoring
138 the occurrence of MnOx containing particles. MnOx production may be microbially mediated
139 (Richardson et al., 1988), or authigenic (Glockzin et al., 2014). In sulfidic waters, the reduction of
140 MnOx with sulfide occurs within a scale of seconds to minutes (Neretin et al., 2003), and is
141 inhibited by nitrate (Dollhopf et al., 2000). The oxygenation of the deep water of GB by the
142 2014/2015 MBI combined with the release of Mn from the sediments into the water column (Lenz
143 et al., 2015) generate appropriate conditions to enhance particulate MnOx formation and
144 vertically expand the zone where they could be observed in the water column.

145 MnOx-containing particles have previously been observed at pelagic redoxclines in the Baltic Sea
146 (Glockzin et al., 2014; Neretin et al., 2003). They are amorphous or star-shaped particles, and
147 occur as single particles or form aggregates with OM (Neretin et al., 2003), specifically with
148 transparent exopolymer particles (TEP) (Glockzin et al., 2014). The sinking velocity (0.76 m d^{-1})
149 of those mixed aggregates containing MnOx and TEP was lower than what was predicted by
150 Stokes law possibly due to their star-shaped morphology and the high OM content. TEP are

151 highly sticky, polysaccharide-rich particles that can enhance particle aggregation rates and the
152 formation of marine snow (Engel, 2000; Logan et al., 1995). Thus, the sinking of MnOx-OM
153 aggregates may contribute to the downward flux of POC. However, high content of TEP relative
154 to more dense particles could reduce the density of marine aggregates and decrease their sinking
155 velocity (Engel and Schartau, 1999). Another type of less studied exopolymer particles are
156 Coomassie stainable particles (CSP), they are protein-containing particles that stain with
157 Coomassie brilliant blue (Long and Azam 1996). Little is known about the characteristics and
158 dynamics of those particles in marine systems and their potential to form aggregates with MnOx
159 had not been studied. Different to TEP, CSP have a limited role on the aggregation of diatoms
160 (Prieto et al., 2002; Cisternas-Novoa et al., 2015), but seem to be important for the aggregation of
161 cyanobacteria (Cisternas-Novoa et al., 2015). Mixed MnOx-OM aggregates may affect the
162 cycling of particle-reactive elements like phosphorus and trace metals via scavenging processes,
163 and it has been proposed that they could act as carriers of bacteria in the redoxcline (Dellwig et
164 al., 2010). To date, there are no measurements of the density of MnOx-OM aggregates, their
165 potential ballast effect on sinking OM, or their biogeochemical role modifying the vertical flux of
166 POM in the Baltic Sea.

167 The objectives of this study are, first, to determine the amount and composition of particles
168 sinking out of the euphotic zone into the deep basins of the Baltic Sea: GB and LD. Second, to
169 study how the oxygenation of deep waters (>140 m) caused by the 2014/2015 MBI may affect the
170 vertical flux of sinking particles. We, therefore, compared GB affected by the MBI with LD that
171 was not affected and exhibited low O₂ concentration (>74 m) and even sulfidic conditions (>180
172 m). We hypothesized that the MBI that altered the water column chemistry and created different
173 O₂ conditions in GB compared with LD affected the composition and vertical flux of sinking
174 particles. Additionally, the higher abundance and *in-situ* formation of MnOx-OM aggregates may
175 cause differences in degradation and export of OM between those two basins.

176 **2. Methods**

177 *2.1. Sampling location and water column properties*

178 Samples were collected during the BalticOM cruise in the Baltic Sea onboard the *RV Alkor* from
179 June 3th to June 19th, 2015. We collected sinking particles using surface-tethered drifting sediment
180 traps (Engel et al., 2017; Knauer et al., 1979) in GB and LD (Table 1). Additionally, water
181 column samples (table 2) were collected using a Niskin-bottle rosette at the locations of the trap
182 deployments. Temperature, salinity and O₂ concentration were determined at each station using a
183 Sea-Bird (CTD) probe equipped with a O₂ sensor (Oxyguard, PreSens), calibrated with discrete
184 samples measured using the Winkler method (Strickland and Parsons, 1968; Wilhelm, 1888).

185 *2.2. Sediment trap design and deployment*

186 We deployed two surface-tethered drifting sediment traps for two days in GB, and one day in LD
187 (Fig.1). Each trap collected particles at four depths: 40 m (two arrays were deployed to evaluate
188 replicability of particle collection), 60 m (55m in LD), 110 m and 180 m (Table 1) to estimate
189 POM fluxes to and within the OMZ. 40 m was considered as the base of the euphotic zone based
190 on PAR measurements conducted during the cruise (data not shown). At each depth, 12 acrylic
191 particle interceptor tubes (PITs) mounted in a PVC cross frame were deployed. Each PIT was
192 equipped with an acrylic baffle at the top to minimize the collection of swimmers (Engel et al.,
193 2017; Knauer et al., 1979). The PITs were 7 cm in diameter and 53 cm in height with an aspect
194 ratio of 7.5 and a collection area of 0.0038 m². The cross frame and PITs were attached to a line
195 that had a bottom weight and a set of surface and subsurface floats. The procedures for PIT
196 preparation and sample recovery followed Engel et al. (2017). Shortly before deployment, each
197 PIT was filled with 1.5 L of seawater previously filtered through a 0.2 µm pore size cartridge. A
198 preservative solution of saline brine (50 g L⁻¹) was added slowly to each PIT underneath the 1.5 L
199 of filtered seawater, carefully keeping the density gradient. The PITs were kept covered until
200 deployment and immediately after recovery to avoid contamination. After recovery, the density
201 gradient was visually verified, and the supernatant seawater was siphoned off the PIT. Then, we
202 pooled together the remaining water, containing the sinking material (~0.6-0.8 L), of 12 tubes per
203 depth into a large container, that we filled-up to 10 L with filtered seawater (between 0.4 and 1.5
204 L) to have the same volume per depth. After that, the samples were screened with a 500 µm mesh

205 to remove swimmers (Conte et al., 2001). Subsequently, samples were split into aliquots that were
206 processed for the different biogeochemical analysis as described in Engel et al. (2017).

207 *2.3. Biogeochemical analysis*

208 Nutrients were measured in seawater samples collected in the deployment stations. Ammonium
209 (detection limit of 0.05 μM) was measured directly on unfiltered seawater samples on board after
210 Solórzano (1969). Phosphate, nitrate, and nitrite (detection limit of 0.04 μM) were filtered
211 through a 0.2 μm pore size and stored frozen until their analysis; samples were measured
212 photometrically with continuous flow analysis on an auto-analyzer (QuAAtro; Seal Analytical)
213 after Grasshoff et al. (1999).

214 Particulate organic carbon (POC), nitrogen (PN), organic phosphorus (POP), and chlorophyll *a*
215 (Chl *a*) were determined as described in Engel et al. (2017). Aliquots, of 100 to 200 mL of the
216 trapped material and 500 mL of the seawater samples, were filtered in duplicate for each
217 parameter at low vacuum (<200 mbar), onto pre-combusted GF/F filters (8h at 500°C). The filters
218 were stored frozen (-20°C) until analysis. Prior analysis, filters for POC-PN determination were
219 exposed to acid fumes (37% hydrochloric acid) to remove carbonates and subsequently dried for
220 12h at 60 °C. POC and PN concentrations were determined using an elemental analyzer (Euro
221 EA, Hechatech) after Sharp (1974).

222 POP was analyzed after Hansen and Koroleff (1999). POP was oxidized to orthophosphate by
223 heating the filters in 40 mL of deionized water (18.2M Ω) with Oxisolv (MERCK 112936) for 30
224 min in a pressure cooker. Orthophosphate was determined spectrophotometrically at 882 nm in a
225 Shimadzu UV-VIS Spectrophotometer UV1201.

226 Chl *a* was analyzed after extraction with 10 mL of 90% acetone, the fluorescence of the samples
227 was measured using a Turner fluorometer (440/685 nm, Turner, 10-AU) according to Strickland
228 et al. (1972). The fluorometer was calibrated with a standard solution of Chl *a* (Sigma-Aldrich C-
229 5753).

230 Biogenic silica (BSi) was determined in aliquots of 50 to 100 mL, filtered in duplicate onto 0.4
231 μm cellulose acetate filters. Samples were stored at -20°C until analysis. For the measurements,

232 filters were digested in NaOH at 85°C for 135 min; the pH was adjusted to 8 with HCl. Silicate
233 was measured spectrophotometrically according to Hansen and Koroleff (2007).

234 Polysaccharide (TEP) and protein (CSP) exopolymer particles, from sediment trap and water
235 column samples were analyzed by microscopy according to Engel (2009). Duplicate aliquots of 5
236 to 20 mL were filtered onto 0.4 µm Nuclepore membrane filters (Whatmann) and stained with 1
237 mL of Alcian Blue solution, a dye that target acidic polysaccharides, for TEP or 1 mL of
238 Coomassie brilliant blue solution, a dye commonly used to stain proteins (Bradford, 1976), for
239 CSP. Filters were transferred onto Cytoclear ® slides and frozen (-20°C) until microscopy
240 analysis. For the analysis, thirty images for each filter were captured under 200x magnification
241 using a light microscope (Zeiss Axio Scope A.1) connected to a color camera (AxioCam MRc).

242 Particle abundance and area were measured semi-automatically using an image analysis system
243 including the WCIF ImageJ software. The RGB was split into three channels: red, blue and green,
244 and the red was used to quantify the amount of TEP and CSP. Additionally, TEP and CSP in
245 water samples from the stations where we deployed sediment traps were analyzed
246 spectrophotometrically (with higher vertical resolution than microscopy) according to Passow and
247 Alldredge (1995) and Cisternas-Novoa et al. (2014), respectively. Concentrations of TEP are
248 reported relative to a xanthan gum standard and expressed in micrograms of xanthan gum
249 equivalents per liter ($\mu\text{g XG eq. L}^{-1}$), and concentrations of CSP are reported relative to a bovine
250 serum albumin standard and expressed in micrograms of bovine serum albumin equivalents per
251 liter ($\mu\text{g BSA eq. L}^{-1}$).

252 MnOx-containing particles have been commonly identified based on their morphology, size and
253 elemental composition, confirmed by scanning electron microscopy (SEM) and energy dispersive
254 x-ray microanalysis (EDX) (Neretin et al., 2003; Glockzin et al., 2014; Dellwig et al., 2010,
255 2018). In this study, we did not measure the elemental composition of the particles. Thus, we
256 identified them as "MnOx-like particles" based on similar morphology, size, and association with
257 organic matter (OM) as MnOx-containing particles previously described in the Baltic Sea (eg.,
258 Neretin et al., 2003 and Glockzin et al., 2014). The abundance and size of MnOx-like particles

259 were determined using particle recognition on filters and imaging processing similar to the
260 method used by Neretin et al. (2003) but without the chemical composition analysis of the
261 particles. For the image analysis, we used the same images as for TEP and CSP analysis and
262 modified image analysis procedure described above as follows: thirty images per filter (200x)
263 were analyzed semi-automatically using ImageJ software. After RGB split, the blue channel
264 pictures were used to quantify MnOx-like particles in the water column and sediment traps. In this
265 manner, the MnOx-like particles were clearly visible with a negligible disruption from TEP or
266 CSP stained blue.

267 Total hydrolyzable amino acids (TAA) were analyzed in unfiltered seawater and trapped material.
268 Samples were stored at -20°C until analysis. Duplicate samples were hydrolyzed at 100 °C in 6N
269 HCl (Suprapur® Hydrochloric acid 30%) and 11 mM ascorbic acid for 20h. Amino acids were
270 separated and measured by high-performance liquid chromatography (HPLC), after derivatization
271 with ortho-phthaldialdehyde using a fluorescence detector (Excitation/Emission 330/445 nm)
272 (Dittmar et al., 2009; Lindroth and Mopper, 1979). TAA concentrations were reported as µM of
273 monomer. The quantitative degradation index (DI) of Dauwe et al. (1999), based on changes in
274 amino acids composition of POM as it undergoes degradation processes, was calculated using the
275 factor coefficient of Dauwe et al. (1999) and the average and standard deviation of the TAA of
276 this data set.

277 Total combined carbohydrates (TCHO) > 1 kDa were determined by HPAEC-PAD according to
278 Engel and Händel (2011). TCHO were analyzed in the unfiltered seawater and sediment trap
279 material. Samples were stored at -20°C until analysis. Prior to analysis, the samples were desalted
280 by membrane dialysis using dialysis tubes with 1 kDa molecular weight cut-off (Spectra Por).
281 Desalination was conducted for 4.5h at 1°C. Then, a 2 mL subsample was sealed with 1.6 mL of
282 1M HCl in pre-combusted glass ampoules and hydrolyzed for 20h at 100°C. After hydrolysis, the
283 subsamples were neutralized by acid evaporation under N₂ atmosphere at 50°C, resuspended with
284 ultrapure Milli-Q water and analyzed on a Dionex 3000 ion chromatography system. TCHO
285 concentrations were reported as µM of monomer.

286 *2.4 Phytoplankton abundance*

287 Phytoplankton composition and abundance at the stations where we deployed sediment traps were
288 evaluated using light microscopy and flow cytometry. Counts of phytoplankton cells $> 5 \mu\text{m}$,
289 were made from 50 mL of fixed samples (Lugol's solution, 1% final concentration). Samples were
290 concentrated using gravitational settling and counted under a Zeiss Axiovert inverted microscope
291 (200x magnification) following the guidelines for determination of phytoplankton species
292 composition, abundance (HELCOM, 2012). The counts were made on either half (cyanobacteria,
293 diatoms, and *Dinophysis sp.*) or two strips (chryptophyta, unidentified dinoflagellates, and
294 chlorophyta) of the chamber. Individual filaments of cyanobacteria were counted in 50 μm length
295 units. The size of the counted phytoplankton species ranged from 10 to 200 μm .

296 Phytoplankton, $<20 \mu\text{m}$, cell abundance was quantified using a flow cytometer (FACSCalibur,
297 Becton, Dickson, Oxford, UK). 2 mL samples were fixed with formaldehyde (1% final
298 concentration) and stored frozen ($-80 \text{ }^\circ\text{C}$) until analysis (two weeks later). Red and orange
299 autofluorescence were used to identify chlorophyll and phycoerythrin cells. Cell counts were
300 determined with CellQuest software (Becton Dickenson); pico- and nanoplankton populations of
301 naturally containing chlorophyll and/or phycoerythrin (*i.e.*, *Synechococcus*) were identified and
302 enumerated.

303 2.5 Statistics

304 Significant differences between two parameters were tested using the Mann-Whitney U-test. The
305 results of statistical analyses were assumed to be significant at p -values < 0.05 . Statistical
306 analyses were performed using Matlab software (MatlabR2014a).

307 3. Results

308 3.1. Biogeochemistry of the water column

309 At both stations, GB and LD, the water column was stratified during the study. In GB, the
310 seasonal thermocline was located between 22 and 37 m, with temperature decreasing rapidly from
311 9.8°C in the surface mix layer to 4.7°C below 37 m (Fig. 2a). Deeper in the water column, a
312 pycnocline (halocline) coincided with the oxycline and was located between 65 m ($S=7.6$) and 80
313 m ($S=10.2$); below 80 m the salinity gradually increased up to 13.5 (220 m). A hypoxic layer (<40

314 $\mu\text{M O}_2$) was located between 74 and 140 m; the core of the OMZ ($<10 \mu\text{M O}_2$) was located
315 between 96 and 125 m. The O_2 concentration increased from $35 \mu\text{M O}_2$ at 140 m to $79 \mu\text{M O}_2$ at
316 220 m (Fig. 2a). In LD, the seasonal thermocline was located between 10 and 39 m, where the
317 temperature decreased gradually from 12°C to 4.0°C (Fig. 2b). The pycnocline was between 55
318 ($S=7.2$) and 75 m ($S=9$) below that the salinity was constant ($S=10.7$) until the bottom of the
319 station (430 m). The O_2 concentration was below the detection limit ($<3 \mu\text{M O}_2$) from 74 m to the
320 deepest point sampled in LD (430 m).

321 The vertical profile of nutrients was different at both stations (Fig. 2). In GB, nitrate concentration
322 increased from below the detection limit in the upper ten meters to $0.17 \mu\text{M}$ at 40 m (Fig. 2a).
323 Concentrations were variable within the OMZ with $6 \mu\text{M}$ in the upper (80 m) and lower oxycline
324 (140 m), and $0.12 \mu\text{M}$ in the core of the OMZ (110 m). Nitrate concentration was $4.8 \mu\text{M}$ in the
325 deepest sample (220 m). Nitrite was below the detection limit in most of the water column except
326 for 60 m ($0.09 \mu\text{M}$) and 110 m ($0.11 \mu\text{M}$). Ammonium increased from $0.14 \mu\text{M}$ in the upper ten
327 meters to $1.15 \mu\text{M}$ at 40 m; concentrations were variable within the OMZ with less than $0.15 \mu\text{M}$
328 in the upper (80 m) and lower oxycline (140 m), and maximum concentration of $3.28 \mu\text{M}$ in the
329 core of the OMZ (110m). Vertical profiles of phosphate and silicate at GB were similar; the
330 concentrations steadily increased from the upper ten meters of the water column ($0.29 \mu\text{M}$ and
331 $10.36 \mu\text{M}$, respectively) to the OMZ ($2.67 \mu\text{M}$ and $39.07 \mu\text{M}$, respectively), and gradually
332 decreased below the OMZ (Fig. 2a). H_2S was not detectable in GB.

333 In LD, nitrate and nitrite concentrations were below the detection limit between the surface and
334 250 m ($<0.04 \mu\text{M}$) (Fig. 2b). Nitrite showed a maximum of $0.22 \mu\text{M}$ at 350 m, and nitrate a
335 maximum of $6.0 \mu\text{M}$ at 400 m. Ammonium concentrations varied between 0.06 and $0.59 \mu\text{M}$ in
336 the upper 70 m and increased to 5.97 and $8.03 \mu\text{M}$ in the OMZ (>74 m). The lowest ammonium
337 concentration ($0.07\mu\text{M}$) was measured in the surface and the highest ($8.03 \mu\text{M}$) at 110 m.

338 Phosphate and silicate concentrations were relatively low within the mixed layer; gradually
339 increased below the pycnocline, and decreased again between 110 and 180 m. Phosphate
340 concentrations varied between 1.5 and $2.5 \mu\text{M}$ in the upper 110 m of the water column, decreased

341 to 0.22 μM at 180 m and increased to 2.7 μM at 430 m (deepest sample). Silicate ranged between
342 25 and 38 μM in the upper 110 m of the water column, decreased to 7.4 μM at 180 m, and
343 increased to 38.9 μM at 430 m. H_2S was detectable below 180 m, with the highest concentration
344 (3.97 μM) at 250 m and the lowest (0.04 μM) between 300 and 350 m (Fig. 2b).

345 *3.2. Particulate organic matter concentration in the water column*

346 Chl *a* concentration in the upper 10 m was slightly higher in GB (1.5-1.7 $\mu\text{g L}^{-1}$, Fig. 3b) than in
347 LD (1.4-1.2 $\mu\text{g L}^{-1}$, Fig. 3e). At both stations, more than 90% of the total smaller phytoplankton
348 (<20 μm , pico- and nanophytoplankton) abundance, determined by flow cytometry, were
349 measured in the upper 60 m, although phytoplankton was detectable in the entire water column.
350 Pico- and nanophytoplankton abundance were 10% higher in GB than in LD (Table 2).

351 Picocyanobacteria determined by phycoerythrin fluorescence accounted for 92% and 96% of the
352 total picophytoplankton abundance in GB and LD, respectively. Picocyanobacteria abundance
353 was 30% higher in GB than in LD.

354 Phytoplankton (>5 μm) abundance, determined by microscopy, was 63% higher in LD than in GB
355 (Table 3). Filamentous cyanobacteria dominated the phytoplankton community at both stations
356 with up to 90% corresponding to *Aphanizomenon* sp. Cyanobacteria represented 56% of the
357 phytoplankton counts in GB and up to 74% in LD. Dinoflagellates (including mixotrophs),
358 dominated by *Dinophysis* sp, were significant in both stations (19% of the phytoplankton counts),
359 whereas chlorophytes (dominated by filaments of *Planctonema* sp. containing cylindrical cells)
360 were more abundant in GB than in LD (25% and 4% of the phytoplankton counts respectively).
361 Diatoms represented less than 1% of the phytoplankton in both stations, and they were slightly
362 more abundant at 40 m in LD (Table 3). BSi was higher in the upper 10 m (0.4-0.5 μM) and
363 decreased with depth in GB (Fig. 3b), whereas in LD, BSi showed a peak at 40 m and then
364 decreased with depth (Fig. 3e).

365 Vertical profiles of POC, PN, and POP concentration were similar in the water column of the two
366 stations (Fig. 3a, d). In GB, the concentrations were higher in the upper 10 m of the water column
367 (POC: 40.38 ± 0.80 , PN: 3.89 ± 0.01 , and POP: 0.26 ± 0.04 μM) and decreased gradually with

368 depth until 110 m where relatively high concentrations (POC 18 ± 0.63 , PN: 2 ± 0.08 , and POP:
369 $0.2 \mu\text{M}$) were observed. The lowest concentrations were found at 180 m (POC: 11.97 ± 1.03 , PN:
370 1.05 ± 0.02 , and POP $< 0.03 \mu\text{M}$) (Fig. 3a). In LD, POM decreased with depth from the surface
371 (POC: 35 ± 0.99 , PN: 4 ± 0.09 , and POP: $0.2 \mu\text{M}$) to 40 m, remained relatively constant between
372 40 and 80 m and decreased again between 110 and 250 m (Fig. 3d).

373 We observed high concentrations of TEP and CSP in the upper 10 m in both stations. The highest
374 TEP concentration was determined at 1 and 10 m at both stations, and it was slightly higher (19%)
375 in GB than in LD (Fig. 3c, f). TEP and CSP vertical profiles were different from each other in GB
376 (Fig. 3c) and covaried in LD (Fig. 3f). Like observed for POC, PN, and POP, TEP concentrations
377 showed a peak at 110 m ($50.29 \pm 6.17 \mu\text{g XG eq. L}^{-1}$) in GB. The highest concentration of CSP at
378 this station was observed in the shallowest (1 m) sample, CSP concentration decreased quickly
379 below 10 m, and then it increased at 140 and 220 m (the deepest sample, approximately 28 m
380 above the seafloor) (Fig. 3c). In LD, the highest concentrations of TEP and CSP were measured at
381 the surface (1 and 10 m) and at 110 m (Fig. 3f). TEP and CSP decreased with depth in the first 80
382 m (from 53.26 ± 7.10 to $18.39 \pm 4.57 \mu\text{g XG eq. L}^{-1}$ and from 53.26 ± 7.10 to $31.57 \pm 18.78 \mu\text{g BSA}$
383 eq. L^{-1}). Both types of gel-like particles showed an increase in concentration at 110 m ($49.25 \pm$
384 $4.08 \mu\text{g XG eq. L}^{-1}$ and $66.89 \pm 22.33 \mu\text{g BSA eq. L}^{-1}$ respectively). Below 110 m, TEP
385 concentrations stayed relatively constant, while CSP concentrations decreased at 180 m and kept
386 relatively constant below that depth.

387 *3.3. MnOx-like particles vertical distribution in the water column*

388 Dark, star-shaped MnOx-like particles (Glockzin et al., 2014; Neretin et al., 2003) were only
389 observed below the fully oxygenated mixed layer in GB and, in less abundance, in LD (Fig. 4). In
390 GB, MnOx-like particles were observed from 80 m to 220 m; they appear as single particles and
391 forming large aggregates containing several MnOx-like particles associated with OM. Relatively
392 high concentration of MnOx-like particles (2×10^6 particles L^{-1}) were observed in the upper (80 m,
393 $25 \mu\text{M O}_2$) and lower (140 m, $36 \mu\text{M O}_2$) oxycline, and at 220 m, $79 \mu\text{M O}_2$ (4×10^6 particles L^{-1})
394 (Fig. 4a). The lowest abundance of MnOx-like particles (7×10^5 particles L^{-1}) was observed at

395 110 m, $6 \mu\text{M O}_2$, i.e. in the core of the OMZ. The equivalent spherical diameter (ESD) of MnOx-
396 like particles varied between 0.6 and $30.5 \mu\text{m}$, with a median size of $3.0 \mu\text{m}$. The largest
397 aggregates (up to $30.5 \mu\text{m}$) were observed in the upper oxycline (80 m). In LD, MnOx-like
398 particles were less abundant, smaller, and had a narrow distribution in the water column than in
399 GB. MnOx-like particles were not detected in the fully oxic (0-40 m) or fully anoxic (180 to 430
400 m) water column. At 60 m ($135 \mu\text{M O}_2$), right above the oxycline, MnOx-like particles began to
401 appear, however, in relatively low abundance. The maximum abundance of MnOx-like particles,
402 $9 \times 10^5 \text{ L}^{-1}$, was observed in the oxycline at 70 m ($27 \mu\text{M O}_2$, Fig. 4b). The ESD ranged between
403 0.6 and $13.4 \mu\text{m}$, the largest aggregates were observed at 70 m.

404 *3.4. Vertical flux of Sinking Particles*

405 Vertical fluxes of POC and PN varied little with depth in GB (Fig. 5a). POC flux slightly
406 increased by 18% from the shallowest (40 m) to the deepest (180 m) sediment trap. Fluxes of PN
407 (Fig. 5a) and CSP (Fig. 6b) were higher at 40 and 60 m and decreased (19 and 70 %) from 60 to
408 180 m respectively. On the other hand, fluxes of POP, BSi, Chl *a* (Fig. 5b) and TEP (Fig. 6a)
409 peaked in the sediment trap located in the core of the OMZ (110 m). The increment of fluxes at
410 110 m coincided with the high abundance of MnOx-like particles associated with TEP (Fig. 6a).
411 In addition, TEP size distribution, determined by image analysis, indicated an increase in large
412 TEP at 110 m (data not shown). In contrast, in LD, POC, PN (Fig. 5c) and CSP (Fig. 6d) fluxes,
413 steadily decreased with depth by 28, 42 and 56% from 40 to 180 m. Similar to the fluxes
414 measured in GB, the POP, BSi (Fig. 5d) and TEP (Fig. 6c) showed a smaller peak in the sediment
415 trap located at 110 m.

416 MnOx-like particles were drastically less abundant in sediment trap samples from LD than in GB,
417 and when present, they appeared as single particles, not aggregated with TEP or CSP (Fig. 6c, d).
418 At both stations, and similar to the water column samples, MnOx-like particles were not observed
419 in sediment trap samples collected in fully oxygenated waters (40 and 60 m). The flux of MnOx-
420 like particles at 110 and 180 m was two orders of magnitude larger in GB than in LD (Table 4). In
421 GB, MnOx-like particles occurred as single particles as well as aggregates with each other and

422 OM such as TEP and CSP (Figure 6a,b, and e), phytoplankton cells, or detrital material. The ESD
423 of MnOx-like particles and aggregates collected in the traps ranged from 0.6 to 167 μm (median
424 2.8 μm) at 110 m and from 0.6 to 153 μm (median 3.3 μm) at 180 m. In LD, only a few, single
425 MnOx-like particles were observed at 110 m (Fig. 6 c, d), their size ranged from 0.6 to 16.5 μm
426 (median 1.8) (Table 4).

427 TAA flux ranged from 371 ± 12 to 501 ± 33 $\mu\text{mol m}^{-2}\text{d}^{-1}$ in GB and from 502 ± 84 to 785 ± 54 μmol
428 $\text{m}^{-2}\text{d}^{-1}$ in LD (Fig. 7a). In GB, the flux steadily decreased from surface to depth, whereas in LD
429 the TAA flux at 40 m was lower than at 60 m and decreased with depth from 60 to 180 m (Fig.
430 7b). The vertical profile of TCHO flux was similar in both stations, although the magnitude of the
431 flux was higher at LD. The TCHO flux varied between 303 ± 8 and 428 ± 14 $\mu\text{mol m}^{-2}\text{d}^{-1}$ in GB
432 (Fig. 7a) and between 503 ± 19 and 584 ± 8 $\mu\text{mol m}^{-2}\text{d}^{-1}$ in LD (Fig. 7b). At both stations, TCHO
433 fluxes increased from 40 to 110 m, where the highest flux was measured, and then it decreased at
434 180 m.

435 *3.5. Chemical composition of sinking and suspended particles*

436 Comparing molar elemental ratios of sinking (from sediment trap material) and suspended (from
437 water column) particles to the revisited Redfield ratio for living plankton (106C: 16N: 15Si: P;
438 Redfield et al., 1963; Brzezinski, 1985), our results showed that the POC:PN ratio of sinking
439 particles was slightly above this ratio at both stations. The POC:PN ratios of sinking particles in
440 GB and LD were not significantly different. In GB however, ratios increased with depth from 9.8
441 to 12.6, while in LD it varied between 11.1 and 15.4 without a clear trend with deep. The
442 POC:POP ratio of sinking particles was lower ($p < 0.05$; Mann–Whitney U-test) in GB (90.1-244)
443 than in LD (230-772) with the highest value observed at 40 m and the lowest at 110 m. At both
444 stations the POC:BSi ratios varied between 1.7 and 4.2 and PN:BSi ratios varied between 0.2 and
445 0.4; the lowest values were observed at 110 m (Table 5).

446 Contrastingly, in suspended particles, POC:PN ratios were higher in GB than in LD ($p < 0.001$). In
447 GB, it varied between 8.4 and 12 without a clear trend with depth; while in LD, it decreased with
448 depth from 8.7 (at 1m) to 6.2 (at 400 m), and a slightly higher value of 7.8 was observed at 430 m.

449 The POC:PN and POC:POP were significantly higher ($p<0.01$) in sinking than in suspended
450 particles (Table 5). The POC:BSi and the PN:BSi ratios were much lower in sinking than in
451 suspended particles at both stations (GB: $p<0.05$; LD: $p<0.01$). In sinking particles, the POC:BSi
452 ratio was below Redfield ratio of 7, whereas it was one to two orders of magnitude higher in
453 suspended particles (Table 5). The PN:POP ratio was significantly lower in sinking (0.15-0.43)
454 than in suspended particles (9.7-44.5) at both stations ($p<0.001$). In sinking particles, it was
455 always below the Redfield ratio of 16, while in suspended particles, it was in the range of
456 Redfield ratio in the upper 80 m in GB and always above in LD.

457 At both stations, the contribution of AA to POC was more significant in sinking than in
458 suspended particles. Similarly, the carbon contained in TCHO made up a larger percentage in
459 sinking than in suspended particles (Table 5). The amino acid-based degradation index (DI,
460 Dauwe et al., 1999) varied from 0.1 to 1.14 in sinking OM and was higher than in suspended OM
461 (-1.25 to -0.42) in both stations. In sinking OM, the DI decreased with depth in GB, whereas in
462 LD, there was not a clear trend with depth (Table 5). The DI was higher in GB than in LD in
463 sinking as well as in suspended OM.

464 **4. Discussion**

465 In this study, we 1) characterized the biogeochemistry of the water column and the sinking
466 particles in GB and LD, during early summer 2015, and 2) determined the vertical flux of sinking
467 particles in those two deep basins of the Baltic Sea. Our results suggested that the intrusion of
468 oxygenated water to GB, as consequence of the 2014/2015 MBI, caused changes in the water
469 chemistry that affected the chemical composition and degradation stage of the sinking and
470 suspended particles. Consequently, the composition and magnitude of the sinking particle flux
471 were different in GB and LD.

472 *4.1 Physical and biogeochemical conditions in GB and LD*

473 In general, physical and biogeochemical conditions (temperature, salinity, O_2 , and inorganic
474 nutrient concentrations) were similar in the euphotic zone of both stations. Moreover, though
475 there were slight differences between the stations concerning phytoplankton abundance and

476 composition, and concentration and chemical composition of POM, in the surface water column,
477 those were not significant. The concentration of Chl *a* (Fig. 3) and the abundance of pico- and
478 nano-phytoplankton (Table 2) were slightly higher (20 and 10 % respectively) in GB than in LD.
479 This agrees with estimates of integrated total primary production (PP), which were 10% higher in
480 GB (380 mg C m⁻² d⁻¹) than in LD (334 mg C m⁻² d⁻¹; Piontek et al., unpublished). At both
481 stations, the abundance of pico-phytoplankton (<2 µm) was an order of magnitude higher than
482 nano-plankton (Table 2). These findings coincided with what was described previously for early
483 summer in the Baltic Sea that indicate that during this period the productivity is sustained mostly
484 by pico- and nano-phytoplankton communities (Leppänen et al., 1995) which co-existed with
485 cyanobacteria and other phytoplankton species (Kreus et al. 2015). Microscopic analysis, on the
486 other hand, indicated that phytoplankton (>5 µm) abundance was 47% higher in LD than in GB.
487 At both stations, filamentous cyanobacteria (> 90% *Aphanizomenon* sp.) were numerically the
488 predominant type (55 and 74% of the phytoplankton counts in GB and LD respectively),
489 dinoflagellates (including mixotrophs) correspond to 20%, and diatoms correspond to >1% of the
490 phytoplankton abundance in the upper 40 m (Table 3). Diatoms were slightly higher in LD than in
491 GB, and this coincide with a small peak in BSi concentration (1.5 µM, Fig. 3e) at 40 m in LD.
492 Although at both stations the diatoms proportion from the total phytoplankton abundance was
493 negligible, they could make a difference in the composition of sinking particles leaving the
494 euphotic zone in LD due to selective aggregation of diatoms (Passow et al., 1991); however, in
495 both stations sinking particles showed a similar enrichment in BSi. The low abundance of diatoms
496 relative to cyanobacteria in the euphotic zone indicated that at both stations, the spring bloom was
497 terminated and cyanobacteria were starting to build up the summer bloom that generally occurs in
498 June-July (Kreus et al., 2015); *Aphanizomenon* sp. and *Nodularia spumigena*, are known to form
499 summer blooms, where they accumulate at the sea surface of the thermally stratified water
500 column (Bianchi et al., 2000; Nausch et al., 2009; Wasmund, 1997).

501 The concentration of particulate elements (POC, PN, POP, BSi) was slightly higher in the surface
502 waters of GB compared to LD; while polysaccharide (TEP) and protein (CSP) containing

503 exopolymeric particles were in similar abundance at both stations. TEP and CSP were more
504 abundant in the euphotic zone, which supports the idea of a phytoplankton origin; however, the
505 concentration of TEP in this study was 69% (in GB) and 76% (in LD) lower than previously
506 reported for summer in the central Baltic Sea (Engel et al., 2002). Likewise, our dissolved
507 inorganic nitrogen concentrations were below the detection limit in the surface, while phosphate
508 concentrations were higher ($>0.3 \mu\text{M}$) than observed in the Engel et al. (2002) study. Mari and
509 Burd (1998) reported that TEP concentration peaked during the spring bloom and in summer in
510 the Kattegat. TEP production may be enhanced by environmental conditions such as nutrient
511 limitation (Mari et al., 2005; Passow, 2002), which are characteristic of late summer in the Baltic
512 Sea (Mari and Burd 1998). In the Baltic Sea, the spring bloom (March-April) is usually followed
513 by a period of reduced PP ($\text{Chl-}a \sim 2 \mu\text{g L}^{-1}$) that preceded the cyanobacteria summer bloom,
514 typically observed in June-July (Kreus et al., 2015). Surface satellite-derived *Chl-a* concentrations
515 (MODIS) in GB indicate a constant increment from mid-May to mid-June 2015 (Le Moigne et al.,
516 2017); our monthly *Chl-a* concentrations derived from VIIRS for June 2015 in the Baltic Sea
517 (Fig.1) showed similar *Chl-a* concentrations. Considering this trend in *Chl-a* concentration and
518 the availability of phosphate in the water column, we could assume that our samples were
519 collected at the beginning of the summer bloom (middle June). In general ecosystem models from
520 the Baltic Sea indicate that the termination of the summer bloom depends upon the phosphate
521 availability (Kreus et al., 2015). Thus, likely TEP concentrations had not reached the higher value
522 previously observed after summer bloom when inorganic nutrients were depleted. Although
523 satellite-derived *Chl-a* concentrations is a valuable tool to evaluate the trend of the PP, the
524 magnitude of the concentration of *Chl-a* from remote sensing is difficult to estimate in the Baltic
525 Sea (Darecki and Stramski, 2004). The concentration of *Chl-a* in GB and LD derived from direct
526 measurements were much lower ($\sim 1.5 \mu\text{g L}^{-1}$), suggesting that our samples were collected during
527 a period of low phytoplankton biomass typically observed before the summer bloom. In any case,
528 the concentration of phosphate was not limiting the system. Another possible explanation for the
529 rather low concentrations of TEP could be their removal from the surface by aggregation and

530 subsequent sedimentation during the spring bloom due to the high abundance of cells and detrital
531 particles during this time (Engel et al., 2002) and the relatively low grazing pressure that lead to
532 higher export after the spring bloom (Lignell et al., 1993).

533 Although the composition and amount of OM in the surface waters at the two trap stations were
534 similar, below the euphotic zone (40 m) the vertical profile of nutrients and particulate matter
535 concentrations were distinctly different; likely due to the 2014/2015 MBI (Holtermann et al.,
536 2017) that reached the deep waters of GB. This inflow replaced the old stagnant water masses by
537 new water masses (Schmale et al., 2016), changing the salinity in the deepest waters and the
538 vertical distribution of O₂ increasing its concentrations below 140 m and constraining the oxygen-
539 deficient layers from 74 to 140 m depth. The combination of physical effects (the displacement of
540 water masses, turbulent mixing and lateral transport) and the consequent development of redox
541 conditions through 2015 may have impacted the distribution of MnOx-like particles and POM in
542 GB. In addition to changes in O₂ concentration, the MBI altered the redox conditions in GB
543 creating a secondary redoxcline at 140 m, where concentrations of O₂ and MnOx-like particles
544 increased. One consequence of those changes is the vertical extension of the layer in which
545 MnOx-containing aggregates could form (Schmale et al., 2016); a previous study showed that
546 MnOx might precipitate from the water column of GB following a MBI event (Lenz et al., 2015).
547 POC and PN concentrations peaked at 110 m, this higher concentration at 110 m was even more
548 evident in POP and TEP, while CSP concentration peaked at 140 m (Fig. 3); this is the first study
549 that examines the potential role of CSP in forming aggregates with MnOx-containing particles.
550 The highest concentration of MnO-like particles (Fig. 4a) in the water column was not observed at
551 110 m (the core of the OMZ) but at 80 m (oxycline), and below 140 m in the newly oxygenated
552 water layers.

553 In contrast, LD maintained permanent suboxic (<5 μM O₂) waters below 74 m as H₂S was
554 detectable below 180 m. Below 100 m the vertical profiles of POM and BSi did not change with
555 depth. The only exception was TEP and CSP concentration that similar to in GB peaked at 110 m
556 and MnOx- like particles showed a small increment at 70 m (in the oxycline). This suggest that,

557 similar to the results of Glockzin et al (2014), the MnOx-like particles, abundant in the oxycline
558 may form sinking aggregates with TEP and CSP, then, when those aggregates sunk to anoxic
559 waters (below 74 m), the MnOx-like particles may dissolve releasing TEP and CSP to the water
560 column, where CSP concentration decreased quickly likely due to microbial degradation, but the
561 concentration of TEP remain constant to the bottom of LD.

562 MBI can have a significant impact on nutrient recycling. In GB nitrate concentration increased
563 possibly as a consequence of the oxidation of reduced nitrogen compounds (e.g., ammonium,
564 ammonia and organic nitrogen compounds like urea) (Le Moigne et al., 2017) that accumulated
565 during the stagnation (anoxic) period previous to the MBI (Hannig et al., 2007). Scavenging of
566 phosphate onto Mn or Fe oxides has been shown in previous studies (Neretin et al., 2003).
567 Phosphate can bind to Fe hydroxides and MnOx and settle down during oxic conditions, building
568 up a phosphate pool in the sediments that later on when the O₂ decreases may become a source of
569 phosphate (Gustafsson and Stigebrandt, 2007). Moreover, Myllykangas et al. (2017) reported that
570 the new water masses intruded during 2014/2015 MBI displaced the stagnant water masses in GB.
571 Thus, the low concentrations of silicate and phosphate that we measured in the deep waters of GB
572 may also be a direct consequence of the intrusion of oxygenated, low-nutrient waters associated
573 with the MBI. In contrast, in LD, the water column remained anoxic down to the sea floor (430
574 m), below the oxycline an increase of ammonium was observed (Fig.2b), which could be an
575 indicator for anaerobic respiration of OM, e.g., denitrification (Bonaglia et al., 2016; Hietanen et
576 al., 2012).

577 In summary, though GB and LD had similar surface conditions in terms of phytoplankton
578 production and POM stocks, during this study, we found differences in the vertical concentration
579 of nutrients (Fig. 2) and POM (Fig. 3) between GB, ventilated by the MBI, and LD, a station that
580 remained suboxic. Our results suggest that the MBI caused differences in the vertical profile of O₂
581 that modified the redox conditions of the water column and enhance the *in-situ* formation of
582 MnOx-like particles (Fig. 4). Alternatively, the inflow may transport new MnOx-like particles to

583 GB. Those abundant MnOx-like particles may aggregate with POM in GB, influencing the
584 vertical distribution of POM in the water column.

585 *4.2 Potential influence of O₂ concentration and redox conditions on vertical flux of sinking*
586 *particles in GB and LD*

587 During this study, we also investigated the effect of different O₂ concentrations and redox
588 conditions on the fluxes of particles. Our measurement of POC flux at 40 m, below the euphotic
589 zone, were 11.7 ± 0.82 mmol C m⁻² d⁻¹ in GB and 19.8 ± 1.22 mmol C m⁻² d⁻¹ in LD. Extrapolating
590 those measurements to annual flux, we obtain 4.37 ± 0.31 mol C m⁻² yr⁻¹ in GB and 7.44 ± 0.46 mol
591 C m⁻² yr⁻¹ in LD. Our results from GB are in the same range as the estimation derived from a
592 biogeochemical model; *i.e.* 3.8 - 4.2 mol C m⁻² yr⁻¹ (Kreus et al., 2015; Sandberg et al., 2000;
593 Stigebrandt, 1991) for the Baltic Sea; however, our results from LD are higher than the annual
594 POC fluxes predicted by those models. The high POC flux observed in this study is not surprising
595 since it represented one (in LD) and two (in GB) days in June when the POC vertical flux out of
596 the euphotic zone is relatively higher in the Baltic Sea compared with late fall and winter. The
597 biogeochemical model of Kreis et al. (personal communication) estimated that POC flux in June
598 ranged between 8 and 13 mmol m⁻² d⁻¹; this is in the same range that our observations.

599 One of the main advantages of our sediment traps is that we can study the flux of sinking particles
600 at various depths simultaneously (*i.e.* higher vertical resolution). Therefore, we measured the
601 POM flux in oxic waters (40 m and 60 (55) m); at the core of the OMZ (110 m) at 180 m in both
602 basins. Traps located a 180 m depth collected particles in sulfidic waters at LD and in recently
603 oxygenated waters (affected by the MBI) in GB. The vertical flux of POM and BSi was different
604 at the two studied basins; for example, POC flux was between 25 and 40% higher in the upper
605 110 m of the LD than in GB (even though the PP was 10% higher in GB). However, the POC
606 fluxes at 180 m (deepest trap) were similar in both basins; indicating a substantial decrease in the
607 POC flux between 110 and 180 m at the LD. The POC flux (and the PN flux which showed a
608 similar vertical profile) did not decrease with depth in the GB. In contrast, in the LD there was a

609 reduction of 17 and 16% of the POC flux from 40 m and 60 m (in the oxycline) and from 110 to
610 180 m respectively; the POC flux did not change from 60 to 110 m when a large section of the
611 water column was suboxic ($O_2 < 5 \mu\text{M}$ from 74 m to the bottom of the station). From 110 to 180
612 m the water column was completely anoxic, and H_2S was detectable at 180 m. The high flux of
613 POC at GB coincided with the appearance of dark, star-shaped particles that we defined as
614 MnOx-like particles, particularly evident at GB (Fig. 6a,b, and e), but also present in LD. Based
615 on their morphology, size, and aggregation with OM, we propose that those particles correspond
616 to MnOx-containing particles enriched in OM that have been previously described at GB (Neretin
617 et al., 2003; Pohl et al., 2004; Glockzin et al., 2014; Dellwig et al., 2010, 2018) and LD (Glockzin
618 et al., 2014; Dellwig et al., 2010). The higher flux of MnOx-like particles in GB than in LD is
619 probably due to the oxygenation and change in the deep water redox conditions that enhance the
620 formation of MnOx-like particles associated with OM. This suggests that the reduction of the
621 POC flux below 110 m in the LD may be related to the O_2 depletion and the absence of MnOx-
622 OM aggregates in the anoxic zone.

623 The POP flux was similar in the oxic water column (up to 60 m) in both basins; however, it was
624 almost two and three times higher at 110 and 180 m respectively in GB than in LD. A peak in the
625 POP and BSi flux was observed at 110 m in both basins, but the magnitude of the increment was
626 much higher GB than in LD. In GB the POP flux increased 62% from 60 to 110 m (OMZ) and
627 then decreased by 28% from 110 to 180 m. Vertical flux of POP, BSi, and Chl-*a* (Fig. 5) were
628 enhanced at 110 m, which coincide with the high flux of MnOx-like particles. This high flux of
629 MnOx-like particles is maintained at 180 m, while the POP, BSi and Chl-*a* flux decreased at this
630 depth. This vertical distribution is likely due to the enhanced formation of MnOx-like particles
631 in the hypoxic layer ($<40 \mu\text{M } O_2$) located between 74 and 140 m that may scavenge POP, and
632 aggregate with cells or phytodetritus containing BSi and Chl-*a*. Although the POP flux peaked at
633 110 m in LD as well, the increment was only 30 % from 60 m (suboxic) to 110 m (anoxic), and it
634 decreased by 78% from 110 to 180 m (sulfidic waters), these variations with depth were also

635 observed in the BSi flux. In LD, the flux and size of MnOx-like particles were much smaller than
636 in GB, and they were more abundant at 110 m than at 180 m.

637 Similar to the vertical distribution of POM in the water column discussed in section 4.1,
638 differences in POM and BSi fluxes between basins are likely associated with the large inflow of
639 oxygen-rich saltwater that displaced the old-stagnant water masses and changed the chemistry of
640 the water column (Mylykangas et al., 2017). Under euxinic conditions (*e.i.*, scenario observed in
641 LD without the influence of the MBI), the maximum concentration of particulate Mn is found in
642 the oxycline (Glockzin et al., 2014). Below the oxycline, and due to the presence of H₂S, the
643 particulate Mn concentration decreased drastically. During this study, we observed a high
644 concentration of MnOx-like particles flux at 110 and 180 m (Table 5) in GB, in agreement with
645 the high flux of particulate Mn measured in sediment traps located at 186 m in June 2015
646 (Dellwig et al., 2018). The oxygenation of the deep water layers of GB by the MBI caused the
647 absence of H₂S (Schmale et al., 2016) and provided redox conditions favorable for the formation
648 of MnOx, resulting in the high MnOx-like particles flux measured in the sediment trap located in
649 the core of the OMZ (110 m) and at 180 m (oxygenated deep water). There were two possible
650 sources of MnOx associated with the 2014/2015 MBI in GB. On the one hand, the lateral
651 transport of low-density aggregates formed by MnOx and OM (Glockzin et al., 2014), and on the
652 other hand, the *in-situ* formation and deposition of MnOx following the oxygenation of the water
653 column (Dellwig et al., 2018). In clear contrast to the oxygenated deep layers of GB, in LD, we
654 measured H₂S below 180 m, this could explain why although those aggregates were present in
655 this station at 110 m, they may dissolve in sulfidic waters, thus, were not as abundant and did not
656 form aggregates with TEP (Fig.6c).

657 The presence of MnOx-like particles in aggregates (Fig 6a) may have implications for the vertical
658 flux of POC, PN and POP in a stratified system with a pelagic redoxcline like the Baltic Sea.
659 Under steady state, the upward diffusion and oxidation rates of the dissolved Mn are balanced by
660 the sinking and dissolution rates of MnOx. During Mn-oxidation, the MnOx could aggregate with
661 POM and trace metals. Then, in the sulfidic waters, slow-sinking MnOx enriched in OM will be

662 dissolved liberating the OM and altering the vertical distribution and the flux of all associated
663 particle elements (Glockzin et al., 2014). This has been previously observed in other anoxic
664 basins; for example, in the Cariaco Basin, total particulate phosphorus reached their maximum
665 flux in sediment traps close to the redoxcline (Benitez-Nelson et al., 2004; Benitez-Nelson et al.,
666 2007). Moreover, even in the anoxic zone, the abundant aggregate associated bacteria (Grossart et
667 al., 2006) could partially or entirely degrade the organic compounds in those particles using NO_3^-
668 or MnOx as an electron acceptor. This may explain why we observed a clear peak in the vertical
669 fluxes of POP, BSi, Chl-*a* (Fig. 3a, b), TEP (Fig. 6a) and TCHO (Fig. 7a) at 110 m, followed by a
670 small decrease at 180 m in GB. In LD a smaller increment in the vertical fluxes of POP, BSi (Fig.
671 3d), TEP (Fig. 6c) and TCHO (Fig. 7b) were also observed. The vertical fluxes of those
672 compounds coincided with the abundance of MnOx-like particles; we assume that the MnOx
673 aggregated not only with TEP as described before (Glockzin et al. 2014) and observed in this
674 study (Fig. 6a), but also with aggregates containing phytoplankton cells and phytodetritus that
675 may enhance POP, BSi, Chl *a*, and TCHO export. On the other hand, nitrogen-rich components of
676 POM like PN (Fig. 3a), TAA (Fig. 7a), and CSP (Fig. 6a) gradually decreased with depth in GB,
677 suggesting that those compounds were less scavenged by MnOx-OM rich aggregates.

678 Primary production (PP) in GB was 10% higher than in LD during our study (Piontek et al.
679 unpublished data). However, the POC flux below the euphotic zone (at 40 m) was 42% higher in
680 LD than in GB and comparable at both stations at 180 m. The fraction of PP exported as POC is
681 termed export production (*e-ratio*) (Buesseler et al., 1992), and it is calculated as the POC flux
682 below the euphotic zone divided by the PP. We calculated the *e-ratio* using ^{14}C -based PP
683 measurements (Piontek et al. unpublished data) and carbon flux at 40 m (shallowest sediment trap
684 depth, considered at the base of the euphotic zone). The *e-ratio* was larger in LD (0.77) compared
685 to GB (0.41); *i.e.*, the percentage of the PP exported as POC below the euphotic zone was 77% in
686 LD versus 41% in GB. This suggests that either a higher proportion of the PP was remineralized
687 in the euphotic zone of GB compared with LD, or particles were sinking faster in LD than in GB
688 likely due to differences in composition. On the other hand, the transfer efficiency of POC to the

689 deeper water column (*i.e.*, the ratio of POC flux at 180 m over POC flux at 40 m) was higher in
690 GB (115%) than in LD (69%). The transfer efficiency of POM is largely controlled by the
691 remineralization rate and the sinking velocity of particles (De La Rocha and Passow, 2007;
692 McDonnell et al., 2015; Trull et al., 2008). The higher POC transfer efficiency in GB than in LD
693 can be attributable to differences in the sinking velocities of the particles in those two stations.
694 Particulate MnOx may sink through the redoxcline in GB (Neretin et al., 2003) acting as ballast
695 material and nucleus for MnOx-OM rich aggregates formation. Those aggregates could have sunk
696 more quickly, limiting the time spent in the water column and the degradation by particle-
697 attached microbes. Assuming that MnOx-like particles had a density between 1.5 and 2.0 g cm⁻³
698 (Glockzin et al., 2014), the largest particles measured at GB (167 μm, Table 4) will have a sinking
699 velocity based on Stokes' law between 508 and 1014 m d⁻¹. If we consider a mixed aggregate that
700 is 50% TEP, density 0.9 g cm⁻³ (Azetsu-Scott and Passow, 2004) and 50% MnOx (density 1.5 g
701 cm⁻³), its density would be 1.2 g cm⁻³, and its theoretical sinking velocity will be 204 m d⁻¹. This
702 indicates that, theoretically, the largest mixed aggregates composed of MnOx and TEP observed
703 in GB could reach 180 m (the location of our deepest sediment trap) in less than one day.
704 However, the average measured sinking velocity of MnOx-containing particles in the laboratory
705 for particles between 2 and 20 μm was 0.76 m d⁻¹, which is significantly lower than the theoretical
706 value (Glockzin et al., 2014). Glockzin et al. (2014) suggested that the star shape and the content
707 of OM were responsible for the lower than predicted sinking velocity. There is no information
708 about the amount of OM relatively to MnOx-containing particles in those mixed aggregates, or
709 how the MnOx to OM ratio may affect the density and sinking velocity of larger aggregates like
710 the ones we observed. Due to the shape and size of MnOx-OM aggregates observed in our study
711 (Fig. 6e), we could assume those are the same type of aggregates described before by Glockzin et
712 al. (2014). Although we did not measure the sinking velocity of those aggregates, we did observe
713 a higher abundance of them associated with TEP at 110 and 180 m in GB than in LD. Thus, the
714 formation of MnOx aggregates rich in OM could represent an additional mechanism (see
715 introduction) to explain why the efficiency of the OM export is different under anoxic than under

716 oxic conditions in the Baltic Sea. The oxygenation of anoxic deep water in GB caused by the
717 2014/2015 MBI, may have led to enhanced precipitation of manganese, iron, and phosphorus
718 particles (Dellwig et al., 2010; Dellwig et al., 2018). For example, the formation of P-rich, metal
719 oxides precipitates occur in the anoxic waters of the Black Sea (Shaffer, 1986) and Cariaco Basin
720 (Benitez-Nelson et al., 2004; Benitez-Nelson et al., 2007) where higher concentration of particulate
721 inorganic and organic phosphorus have been observed in sediment traps close to the redoxcline.

722 Alternatively, BSi could also act as ballast material incrementing the sinking velocity of marine
723 aggregates (Armstrong et al., 2001; Klaas and Archer, 2002). Our results showed that sinking
724 particles were strongly enriched in BSi relatively to C and N and compared to suspended particles
725 that were depleted in BSi (Table 5). Diatoms are the major phytoplankton group that produces
726 BSi to build their cell walls (Martin-Jézéquel et al., 2000), and they are the dominant
727 phytoplankton species during the spring bloom. However, during our study, diatoms represented
728 less than 1% of the phytoplankton abundance in the water column, and even though there was a
729 strong enrichment in BSi in the sinking particles, this was similar in GB and LD (Table 5).

730 Therefore, either the differences in export production nor in transfer efficiency between GB and
731 LD could not be solely explained by the amount of diatoms cells, phytodetritus or BSi in sinking
732 particles at those two basins.

733 *4.3 Differences on composition and lability of sinking and suspended organic matter in GB and* 734 *LD*

735 In the sections above we compared the biogeochemical conditions and the size of the POM pool
736 in the euphotic zone of GB and LD. We then looked at how the sinking flux of OM was affected
737 by the different O₂ concentrations in the water column. Now, we focus on the influence of O₂ in
738 the chemical composition of sinking and suspended particles. Suspended or slow sinking particles
739 that spend more time in the water column should theoretically, show a more substantial degree of
740 degradation (Goutx et al., 2007). Relative to the Redfield molar ratio: 106 POC:16 PN:15 BSi:
741 POP. POM showed enrichment in POC relative to PN and POP, especially in sinking particles

742 from LD and suspended particles from GB. Our measured values of POC:PN (~10) and POC:POP
743 (between 89 and 506) in suspended OM coincide with the simulated ratio reported immediately
744 after the culmination of the spring bloom by Kreuz et al. (2015). The same study had suggested
745 that POC:POP higher than Redfield ratio might lead to an enhancement of particle export (Kreuz
746 et al., 2015), however, no direct observations had confirmed this hypothesis. Our measurements
747 showed that the relative higher POC:POP ratios in sinking OM from LD, compared with GB, do
748 not lead to a higher transfer efficiency at this station. Compared to the suspended OM in LD, the
749 POP content was lower in GB, possible related to scavenging of POP into MnOx aggregates (see
750 section 3.4).

751 In addition, at both stations, sinking particles were strongly enriched in BSi (Table 5) probably
752 due to the preferential sinking of diatoms and remnants diatom-rich detritus from the spring
753 bloom. Differently, suspended particles had a relatively low content of BSi; this is not surprising
754 considering the small proportions of diatoms in the euphotic zone at the time of our sampling. The
755 concentration of BSi decreased below the detection limit from 60 m in the GB, and 70 m in the
756 LD. This observation coincides with previous studies reporting selective incorporation of diatoms
757 into sinking aggregates in the Baltic Sea (Engel et al., 2002; Passow, 1991), whereas non-diatoms
758 species, although they may be abundant in the suspended phytoplankton, may not be present in
759 sinking particles (Passow, 1991).

760 Another explanation for of higher BSi content in sinking particles may be the inclusion of
761 lithogenic Si in our measurements; lithogenic Si may have been present in the water column or
762 being transported by laterally advected material. A recent study suggests that contributions of non-
763 biogenic sources could be significant during alkaline extraction (Barão et al., 2015). The even
764 more substantial enrichment in BSi observed in sinking particles from 110 m in both basins, may
765 result from adsorption and/or co-precipitation of silica in sinking particles containing MnOx
766 (Dellwig et al., 2010; Hartmann, 1985); or by the formation of aggregates that are enriched in
767 MnOx as well as in phytodetritus from diatom origin.

768 The TAA based degradation index, DI (Dauwe et al. 1999) covers a wide range of alteration
769 stages; the more negative the DI, the more degraded the samples, positive DI indicates fresh
770 organic matter. In our study, the sediment trap material had a DI between 0.10 and 1.14, while
771 suspended OM has a DI between -0.26 and -1.25 (Table 5). These values coincide with what
772 reported earlier by Dauwe et al. (1999), and indicate that: first, the sinking particles collected in
773 the sediment traps were less altered (they have a more positive DI) than the suspended OM
774 collected in the Niskin bottle. Second, sinking particles from GB were fresher than the ones from
775 LD, and the degradation stage increased with depth in both stations. The higher contribution of
776 AA and CHO to the POC pool in sinking than in suspended OM and the AA- DI indicates that
777 suspended OM was more degraded than sinking OM. The highest degree of degradation in
778 suspended OM and sinking OM from LD may be the result of a long time that light suspended
779 OM or slow sinking particles spend exposed to degradation in fully oxygenated surface waters
780 than dense, fast sinking particles collected in sediment traps.

781 The higher abundance of aggregates, formed by a combination of MnOx-like particles and OM,
782 observed at 110 and 180 m in GB could act as bacteria hot spots that combined with a higher O₂
783 concentration in GB may increase the microbial degradation on sinking particles collected in GB.
784 However, the AA-DI, indicated that sinking OM was less altered, and therefore more labile than
785 the sinking OM in LD. This implied that in addition to the higher transfer efficiency of POC in
786 GB (see discussion above); the OM reaching the seafloor was fresher and less degraded. This
787 supports the idea that mix aggregates composed by MnOx and OM may be larger and faster
788 sinking than the previously described by Glockzin et al. (2014). This explanation is mostly
789 speculative, and based on the observation of large mixed aggregates in the 110 and 180 m traps
790 (Fig. 6, Table 4). However, as mention in the previous section, further work on directly
791 determining sinking velocity is required to prove this hypothesis.

792 **Conclusion**

793 Fluxes and composition of sinking particles were different in two deep basins in the Baltic Sea:
794 GB and LD during early summer 2015. The two stations had similar surface characteristics and
795 POM stock; however, at depth, the vertical profile of the POM concentration, as well as the
796 vertical flux of sinking particles was different, likely related to differences in the O₂
797 concentration. The 2014/2015 MBI supplied oxygen-rich waters to GB transporting solid material
798 from shallower areas and modifying the O₂ vertical profile and the redox conditions in the
799 otherwise permanent suboxic deep waters. This event did not affect LD allowing for the
800 comparison of POM fluxes and composition under two different O₂ concentrations with similar
801 surface water conditions. Export efficiency (*e-ratio*) derived from *in-situ* PP measurements and
802 POC flux derivate from sediment traps indicated higher export efficiency in LD than in GB.
803 However, the transfer efficiency (POC flux at 180 m over POC flux at 40 m) suggested that under
804 anoxic conditions found in LD, a smaller portion of the POC exported below the euphotic zone
805 was transferred to 180 m than under oxygenated conditions present in GB. The MBI also transport
806 solid Mn from shallower areas towards GB deep that may have contributed to the higher
807 abundance of MnOx-OM in GB. Our results suggest that a new possible mechanism to explain the
808 differences in the OM fluxes under different O₂ concentration could be the formation and
809 prevalence of aggregates composed of MnOx and organic matter in GB. Those aggregates were
810 significantly larger and more abundant in GB compared to LD where sulfidic waters constrained
811 their presence. Our results indicate that at GB not only a higher proportion of the POM leaving
812 the euphotic zone reached our deepest sediment trap, but also that this POM was fresher and less
813 degraded. We propose that after a MBI in GB, the aggregates containing MnOx-like particles and
814 organic matter could have reached the sediments relatively fast and unaltered, scavenging not
815 only phosphorus and TEP, as described previously, but also other compounds like BSi, POP and
816 CSP. The higher fraction of sinking particles exported below the euphotic zone and reaching 180
817 m in GB suggest that at this station a significant fraction of the POM could reach the sediments,
818 50 m below our deepest sediment trap, relatively unaltered. The remineralization of the organic
819 matter reaching the sediments may contribute to the quick re-establishment of anoxic conditions
820 in the sediment-water interface in GB. The relevance of this process needs to be further

821 investigated in order to be included in O₂ budget and long-term predictions of the MBI impact in
822 the O₂ and OM cycles.

823 **Author Contributions**

824 C.C.N. designed and performed the sediment trap work at sea, analyzed samples and wrote the
825 manuscript. F.A.C.L.M, designed and performed the sediment trap work at sea and contributed to
826 the writing of the manuscript. A.E designed and participated in the scientific program at sea and
827 discussed and commented on the manuscript.

828 **Acknowledgements**

829 This research was supported by the DFG Collaborative Research Center 754 “Climate-
830 Biogeochemistry Interactions in the Tropical Ocean” (to A.E., C.C.N. and F.A.C.L.M), by a
831 Fellowship of the Excellence Cluster ‘The Future Ocean’ (CP1403 to F.A.C.L.M.), and by a
832 DAAD short term grant (57130097 to C.C.N.). We thank Jon Roa, Tania Klüver, Scarlett Sett,
833 Angela Stippkugel, Carola Wagner, Clarissa Karthäuser, Moritz Ehrlich, Sonja Endres, Hannes
834 Wagner, Ruth Flerus, Sven Sturm and Christian Begler for support during traps preparation and
835 deployments, help with experiment or analyzed samples. We Thank Judith Piontek for her
836 contribution to the design of the scientific program at sea, Jaime Soto- Neira for useful discussion
837 and help with figure preparation and Cindy Lee for helpful advices.

References

- Andersen, J. H., Carstensen, J., Conley, D. J., Dromph, K., Fleming-Lehtinen, V., Gustafsson, B. G., Josefson, A. B., Norkko, A., Villnäs, A., and Murray, C.: Long-term temporal and spatial trends in eutrophication status of the Baltic Sea, *Biological Reviews*, 92, 135-149, 2017.
- Armstrong, R. A., Lee, C., Hedges, J. I., Honjo, S., and Wakeham, S. G.: A new, mechanistic model for organic carbon fluxes in the ocean based on the quantitative association of POC with ballast minerals, *Deep Sea Research Part II: Topical Studies in Oceanography*, 49, 219-236, 2002.
- Azetsu-Scott, K. and Passow, U.: Ascending marine particles: Significance of transparent exopolymer particles (TEP) in the upper ocean, *Limnology and Oceanography*, 49, 741-748, 2004.
- Barão, L., Vandevenne, F., Clymans, W., Frings, P., Ragueneau, O., Meire, P., Conley, D. J., and Struyf, E.: Alkaline-extractable silicon from land to ocean: A challenge for biogenic silicon determination, *Limnology and Oceanography: Methods*, 13, 329-344, 2015.
- Benitez-Nelson, C. R., O'Neill, L., Kolowitz, L. C., Pellechia, P., and Thunel, I. R.: Phosphonates and particulate organic phosphorus cycling in an anoxic marine basin, *Limnology and Oceanography*, 49, 1593-1604, 2004.
- Benitez-Nelson, C. R., O'Neill Madden, L. P., Styles, R. M., Thunell, R. C., and Astor, Y.: Inorganic and organic sinking particulate phosphorus fluxes across the oxic/anoxic water column of Cariaco Basin, Venezuela, *Marine Chemistry*, 105, 90-100, 2007.
- Bianchi, T. S., Engelhaupt, E., Westman, P., Andrén, T., Rolff, C., and Elmgren, R.: Cyanobacterial blooms in the Baltic Sea: Natural or human-induced?, *Limnology and Oceanography*, 45, 716-726, 2000.
- Bonaglia, S., Klawonn, I., Brabandere, L. D., Deutsch, B., Thamdrup, B., and Brüchert, V.: Denitrification and DNRA at the Baltic Sea oxic–anoxic interface: Substrate spectrum and kinetics, *Limnology and Oceanography*, 61, 1900-1915, 2016.
- Boyd, P. W. and Trull, T. W.: Understanding the export of biogenic particles in oceanic waters: Is there consensus?, *Progress in Oceanography*, 72, 276-312, 2007.
- Bradford, M. M.: A rapid and sensitive method for the quantitation of microgram quantities of protein utilizing the principle of protein-dye binding, *Analytical Biochemistry*, 72, 248-254, 1976.
- Brettar, I. and Rheinheimer, G.: Denitrification in the Central Baltic: evidence for H_2S oxidation as motor of denitrification at the oxic-anoxic interface, *Marine Ecology Progress Series*, 77, 157-169, 1991.
- Buesseler, K. O., Bacon, M. P., Kirk Cochran, J., and Livingston, H. D.: Carbon and nitrogen export during the JGOFS North Atlantic Bloom experiment estimated from ^{234}Th : ^{238}U disequilibria, *Deep Sea Research Part A. Oceanographic Research Papers*, 39, 1115-1137, 1992.
- Carstensen, J., Andersen, J. H., Gustafsson, B. G., and Conley, D. J.: Deoxygenation of the Baltic Sea during the last century, *Proceedings of the National Academy of Sciences*, 111, 5628-5633, 2014a.
- Carstensen, J., Conley, D. J., Bonsdorff, E., Gustafsson, B. G., Hietanen, S., Janas, U., Jilbert, T., Maximov, A., Norkko, A., Norkko, J., Reed, D. C., Slomp, C. P., Timmermann, K., and Voss, M.: Hypoxia in the Baltic Sea: Biogeochemical Cycles, Benthic Fauna, and Management, *AMBIO*, 43, 26-36, 2014b.
- Cavan, E. L., Trimmer, M., Shelley, F., and Sanders, R.: Remineralization of particulate organic carbon in an ocean oxygen minimum zone, *Nature Communications*, 8, 14847, 2017.
- Cisternas-Novoa, C., Lee, C., and Engel, A.: A semi-quantitative spectrophotometric, dye-binding assay for determination of Coomassie Blue stainable particles, *Limnology and Oceanography: Methods*, 12, 604-616, 2014.
- Conley, D. J., Björck, S., Bonsdorff, E., Carstensen, J., Destouni, G., Gustafsson, B. G., Hietanen, S., Kortekaas, M., Kuosa, H., Markus Meier, H. E., Müller-Karulis, B., Nordberg, K., Norkko, A., Nürnberg, G., Pitkänen, H., Rabalais, N. N., Rosenberg, R., Savchuk, O. P., Slomp, C. P., Voss, M., Wulff, F., and Zillén, L.: Hypoxia-Related Processes in the Baltic Sea, *Environmental Science & Technology*, 43, 3412-3420, 2009.

Conte, M. H., Ralph, N., and Ross, E. H.: Seasonal and interannual variability in deep ocean particle fluxes at the Oceanic Flux Program (OFP)/Bermuda Atlantic Time Series (BATS) site in the western Sargasso Sea near Bermuda, *Deep Sea Research Part II: Topical Studies in Oceanography*, 48, 1471-1505, 2001.

Darecki, M. and Stramski, D.: An evaluation of MODIS and SeaWiFS bio-optical algorithms in the Baltic Sea, *Remote Sensing of Environment*, 89, 326-350, 2004.

Dauwe, B., Middelburg, J. J., Herman, P. M. J., and Heip, C. H. R.: Linking diagenetic alteration of amino acids and bulk organic matter reactivity, *Limnology and Oceanography*, 44, 1809-1814, 1999.

De La Rocha, C. L. and Passow, U.: Factors influencing the sinking of POC and the efficiency of the biological carbon pump, *Deep Sea Research Part II: Topical Studies in Oceanography*, 54, 639-658, 2007.

Dellwig, O., Leipe, T., März, C., Glockzin, M., Pollehne, F., Schnetger, B., Yakushev, E. V., Böttcher, M. E., and Brumsack, H.-J.: A new particulate Mn–Fe–P-shuttle at the redoxcline of anoxic basins, *Geochimica et Cosmochimica Acta*, 74, 7100-7115, 2010.

Dellwig, O., Schnetger, B., Brumsack, H.-J., Grossart, H.-P., and Umlauf, L.: Dissolved reactive manganese at pelagic redoxclines (part II): Hydrodynamic conditions for accumulation, *Journal of Marine Systems*, 90, 31-41, 2012.

Dellwig, O., Schnetger, B., Meyer, D., Pollehne, F., Häusler, K., and Arz, H. W.: Impact of the Major Baltic Inflow in 2014 on Manganese Cycling in the Gotland Deep (Baltic Sea), *Frontiers in Marine Science*, 5, 2018.

Devol, A. H. and Hartnett, H. E.: Role of the oxygen-deficient zone in transfer of organic carbon to the deep ocean, *Limnology and Oceanography*, 46, 1684-1690, 2001.

Dittmar, T., Cherrier, J., and Ludwiczowski, K. U.: The analysis of amino acids in seawater. In: *Practical guidelines for the analysis of seawater* Wurl, O. and Raton, B. (Eds.), CRC Press, 2009.

Dollhopf, M. E., Nealson, K. H., Simon, D. M., and Luther, G. W.: Kinetics of Fe(III) and Mn(IV) reduction by the Black Sea strain of *Shewanella putrefaciens* using in situ solid state voltammetric Au/Hg electrodes, *Marine Chemistry*, 70, 171-180, 2000.

Dugdale, R. C. and Goering, J. J.: Uptake Of New And Regenerated Forms Of Nitrogen In Primary Productivity, *Limnology and Oceanography*, 12, 196-206, 1967.

Emeis, K. C., Struck, U., Leipe, T., Pollehne, F., Kunzendorf, H., and Christiansen, C.: Changes in the C, N, P burial rates in some Baltic Sea sediments over the last 150 years—relevance to P regeneration rates and the phosphorus cycle, *Marine Geology*, 167, 43-59, 2000.

Engel, A.: The role of transparent exopolymer particles (TEP) in the increase in apparent particle stickiness (α) during the decline of a diatom bloom, *Journal of Plankton Research*, 22, 485-497, 2000.

Engel, A., Meyerhöfer, M., and von Bröckel, K.: Chemical and Biological Composition of Suspended Particles and Aggregates in the Baltic Sea in Summer (1999), *Estuarine, Coastal and Shelf Science*, 55, 729-741, 2002.

Engel, A. and Schartau, M.: Influence of transparent exopolymer particles (TEP) on sinking velocity of *Nitzschia closterium* aggregates, *Marine Ecology Progress Series*, 182, 69-76, 1999.

Engel, A., Wagner, H., Le Moigne, F. A. C., and Wilson, S. T.: Particle export fluxes to the oxygen minimum zone of the eastern tropical North Atlantic, *Biogeosciences*, 14, 1825-1838, 2017.

Eppley, R. W. and Peterson, B. J.: Particulate organic matter flux and planktonic new production in the deep ocean, *Nature*, 282, 677, 1979.

Glockzin, M., Pollehne, F., and Dellwig, O.: Stationary sinking velocity of authigenic manganese oxides at pelagic redoxclines, *Marine Chemistry*, 160, 67-74, 2014.

Goutx, M., Wakeham, S. G., Lee, C., Duflo, S. M., Guigue, C., Liu, Z., Moriceau, B., Sempère, R., Tedetti, M., and Xue, J.: Composition and degradation of marine particles with different settling velocities in the northwestern Mediterranean Sea, *Limnology and Oceanography*, 52, 1645-1664, 2007.

Grossart, H. P., Kiørboe, T., Tang, K. W., Allgaier, M., Yam, E. M., and Ploug, H.: Interactions between marine snow and heterotrophic bacteria: aggregate formation and microbial dynamics, *Aquatic Microbial Ecology*, 42, 19-26, 2006.

Gustafsson, B. G. and Stigebrandt, A.: Dynamics of nutrients and oxygen/hydrogen sulfide in the Baltic Sea deep water, *Journal of Geophysical Research: Biogeosciences*, 112, 2007.

Hannig, M., Lavik, G., Kuypers, M. M. M., Woebken, D., Martens-Habbena, W., and Jürgens, K.: Shift from denitrification to anammox after inflow events in the central Baltic Sea, *Limnology and Oceanography*, 52, 1336-1345, 2007.

Hansen, H. P. and Koroleff, F.: Determination of nutrients. In: *Methods of Seawater Analysis*, Wiley-VCH Verlag GmbH, 2007.

Hansen, H. P. and Koroleff, F.: Determination of nutrients. In: *Methods of Seawater Analysis*, Grasshoff, K., Kremling, K., and Ehrhardt, M. (Eds.), Wiley-VCH, Weinheim, Germany, 1999.

Hartmann, M.: Atlantis-II Deep geothermal brine system. Chemical processes between hydrothermal brines and Red Sea deep water, *Marine Geology*, 64, 157-177, 1985.

HELCOM: Guidelines for monitoring phytoplankton species composition, abundance and biomass. In: *Manual for Marine Monitoring in the COMBINE*

Programme of HELCOM, Helsinki Commission, Helsinki 2012.

Hietanen, S., Jäntti, H., Buizert, C., Jürgens, K., Labrenz, M., Voss, M., and Kuparinen, J.: Hypoxia and nitrogen processing in the Baltic Sea water column, *Limnology and Oceanography*, 57, 325-337, 2012.

Holtermann, P. L., Prien, R., Naumann, M., Mohrholz, V., and Umlauf, L.: Deepwater dynamics and mixing processes during a major inflow event in the central Baltic Sea, *Journal of Geophysical Research: Oceans*, 122, 6648-6667, 2017.

Keil, R. G., Neibauer, J. A., Biladeau, C., van der Elst, K., and Devol, A. H.: A multiproxy approach to understanding the "enhanced" flux of organic matter through the oxygen-deficient waters of the Arabian Sea, *Biogeosciences*, 13, 2077-2092, 2016.

Knauer, G. A., Martin, J. H., and Bruland, K. W.: Fluxes of particulate carbon, nitrogen, and phosphorus in the upper water column of the northeast Pacific, *Deep Sea Research Part A. Oceanographic Research Papers*, 26, 97-108, 1979.

Kreus, M., Schartau, M., Engel, A., Nausch, M., and Voss, M.: Variations in the elemental ratio of organic matter in the central Baltic Sea: Part I—Linking primary production to remineralization, *Continental Shelf Research*, 100, 25-45, 2015.

Kullenberg, G. and Jacobsen, T. S.: The Baltic Sea: an outline of its physical oceanography, *Marine Pollution Bulletin*, 12, 183-186, 1981.

Le Moigne, F. A. C., Cisternas-Novoa, C., Piontek, J., Maßmig, M., and Engel, A.: On the effect of low oxygen concentrations on bacterial degradation of sinking particles, *Scientific Reports*, 7, 16722, 2017.

Legendre, L. and Gosselin, M.: New production and export of organic matter to the deep ocean: Consequences of some recent discoveries, *Limnology and Oceanography*, 34, 1374-1380, 1989.

Leipe, T., Tauber, F., Vallius, H., Virtasalo, J., Uścińowicz, S., Kowalski, N., Hille, S., Lindgren, S., and Myllyvirta, T.: Particulate organic carbon (POC) in surface sediments of the Baltic Sea, *Geo-Marine Letters*, 31, 175-188, 2011.

Lenz, C., Jilbert, T., Conley, D. J., Wolthers, M., and Slomp, C. P.: Are recent changes in sediment manganese sequestration in the euxinic basins of the Baltic Sea linked to the expansion of hypoxia?, *Biogeosciences*, 12, 4875-4894, 2015.

Lignell, R. R., Heiskanen, A.-S., Kuosa, H., Kuuppo-Leinikki, P., Pajuniemi, R., and Uitto, A.: Fate of phytoplankton spring bloom: Sedimentation and carbon flow in the planktonic food web in the northern Baltic, *Marine Ecology. Progress Series*, 94, 13, 1993.

Lindroth, P. and Mopper, K.: High performance liquid chromatographic determination of subpicomole amounts of amino acids by precolumn fluorescence derivatization with o-phthalaldehyde, *Analytical Chemistry*, 51, 1667-1674, 1979.

Logan, B. E., Passow, U., Alldredge, A. L., Grossartt, H.-P., and Simont, M.: Rapid formation and sedimentation of large aggregates is predictable from coagulation rates (half-lives) of transparent exopolymer particles (TEP), *Deep Sea Research Part II: Topical Studies in Oceanography*, 42, 203-214, 1995.

Mari, X. and Burd, A.: Seasonal size spectra of transparent exopolymeric particles (TEP) in a coastal sea and comparison with those predicted using coagulation theory, *Marine Ecology Progress Series*, 163, 13, 1998.

Mari, X., Rassoulzadegan, F., Brussaard, C. P. D., and Wassmann, P.: Dynamics of transparent exopolymeric particles (TEP) production by *Phaeocystis globosa* under N- or P-limitation: a controlling factor of the retention/export balance, *Harmful Algae*, 4, 895-914, 2005.

Martin-Jézéquel, V., Hildebrand, M., and Brzezinski, M. A.: SILICON METABOLISM IN DIATOMS: IMPLICATIONS FOR GROWTH *Journal of Phycology*, 36, 821-840, 2000.

Matthäus, W. and Franck, H.: Characteristics of major Baltic inflows—a statistical analysis, *Continental Shelf Research*, 12, 1375-1400, 1992.

McDonnell, A. M. P., Boyd, P. W., and Buesseler, K. O.: Effects of sinking velocities and microbial respiration rates on the attenuation of particulate carbon fluxes through the mesopelagic zone, *Global Biogeochemical Cycles*, 29, 175-193, 2015.

Myllykangas, J. P., Jilbert, T., Jakobs, G., Rehder, G., Werner, J., and Hietanen, S.: Effects of the 2014 major Baltic inflow on methane and nitrous oxide dynamics in the water column of the central Baltic Sea, *Earth Syst. Dynam.*, 8, 817-826, 2017.

Nausch, M., Nausch, G., Lass, H. U., Mohrholz, V., Nagel, K., Siegel, H., and Wasmund, N.: Phosphorus input by upwelling in the eastern Gotland Basin (Baltic Sea) in summer and its effects on filamentous cyanobacteria, *Estuarine, Coastal and Shelf Science*, 83, 434-442, 2009.

Neretin, L. N., Pohl, C., Jost, G., Leipe, T., and Pollehne, F.: Manganese cycling in the Gotland Deep, Baltic Sea, *Marine Chemistry*, 82, 125-143, 2003.

Passow, U.: Production of transparent exopolymer particles (TEP) by phyto- and bacterioplankton, *Marine Ecology Progress Series*, 236, 12, 2002.

Passow, U.: Species-specific sedimentation and sinking velocities of diatoms, *Marine Biology*, 108, 449-455, 1991.

Passow, U. and Alldredge, A. L.: A dye-binding assay for the spectrophotometric measurement of transparent exopolymer particles (TEP), *Limnology and Oceanography*, 40, 1326-1335, 1995.

Richardson, L. L., Aguilar, C., and Neilson, K. H.: Manganese oxidation in pH and O₂ microenvironments produced by phytoplankton^{1,2}, *Limnology and Oceanography*, 33, 352-363, 1988.

Sandberg, J., Elmgren, R., and Wulff, F.: Carbon flows in Baltic Sea food webs — a re-evaluation using a mass balance approach, *Journal of Marine Systems*, 25, 249-260, 2000.

Schmale, O., Krause, S., Holtermann, P., Power Guerra, N. C., and Umlauf, L.: Dense bottom gravity currents and their impact on pelagic methanotrophy at oxic/anoxic transition zones, *Geophysical Research Letters*, 43, 5225-5232, 2016.

Shaffer, G.: Phosphate pumps and shuttles in the Black Sea, *Nature*, 321, 515, 1986.

Stigebrandt, A.: Computations of oxygen fluxes through the sea surface and the net production of organic matter with application to the Baltic and adjacent seas, *Limnology and Oceanography*, 36, 444-454, 1991.

Strickland, J. D. and Parsons, T. R.: Determination of dissolved oxygen. In: *A Practical Handbook of Seawater Analysis*, Fisheries Research Board of Canada, 1968.

Strickland, J. D. H., Parsons, T. R., and Strickland, J. D. H.: *A practical handbook of seawater analysis*, Fisheries Research Board of Canada, Ottawa, 1972.

Thomas, H. and Schneider, B.: The seasonal cycle of carbon dioxide in Baltic Sea surface waters, *Journal of Marine Systems*, 22, 53-67, 1999.

Trull, T. W., Bray, S. G., Buesseler, K. O., Lamborg, C. H., Manganini, S., Moy, C., and Valdes, J.: In situ measurement of mesopelagic particle sinking rates and the control of carbon transfer to the ocean

interior during the Vertical Flux in the Global Ocean (VERTIGO) voyages in the North Pacific, *Deep Sea Research Part II: Topical Studies in Oceanography*, 55, 1684-1695, 2008.

Turner, J. T.: Zooplankton fecal pellets, marine snow, phytodetritus and the ocean's biological pump, *Progress in Oceanography*, 130, 205-248, 2015.

van Hulst, M., Middag, R., Dutay, J. C., de Baar, H., Roy-Barman, M., Gehlen, M., Tagliabue, A., and Sterl, A.: Manganese in the west Atlantic Ocean in the context of the first global ocean circulation model of manganese, *Biogeosciences*, 14, 1123-1152, 2017.

Van Mooy, B. A. S., Keil, R. G., and Devol, A. H.: Impact of suboxia on sinking particulate organic carbon: Enhanced carbon flux and preferential degradation of amino acids via denitrification, *Geochimica et Cosmochimica Acta*, 66, 457-465, 2002.

Wasmund, N.: Occurrence of cyanobacterial blooms in the Baltic sea in relation to environmental conditions, *Internationale Revue der gesamten Hydrobiologie und Hydrographie*, 82, 169-184, 1997.

Wasmund, N. and Uhlig, S.: Phytoplankton trends in the Baltic Sea, *ICES Journal of Marine Science*, 60, 2003.

Wilhelm, W. L.: Die Bestimmung des im Wasser gelösten Sauerstoffes, *Berichte der deutschen chemischen Gesellschaft*, 21, 2843-2854, 1888.

Figure Captions

Figure 1. Monthly averaged Chl *a* distribution derived from VIIRS for June 2015 in the Baltic Sea. Black circle and “x” indicate the position of the trap deployment and the seawater collection, respectively, in Gotland Deep (GB) and Landsort Deep (LD). The lower panel shows the trajectory of the trap deployed at GB and LD.

Figure 2. Water column profiles at the location of the sediment trap deployments in (A) GB, and (B) LD. Left panel: oxygen (blue), temperature (red), and salinity (black). Middle panel: nitrate (NO₃, white squares), nitrite (NO₂, grey circles), and ammonium (NH₄, black triangles). Right panel: phosphate (PO₄, grey diamond), and silicate (Si(OH)₄, black circles). Grey lines indicate the depths at which we deployed sediment traps.

Figure 3. Vertical profiles of concentration of particulate organic carbon (POC), particulate nitrogen (PN), and particulate organic phosphorus (POP) in GB (A) and LD (D); vertical profiles of concentration of chlorophyll *a* (Chl *a*) and biogenic silicate (BSi) in GB (B) and LD (D); and vertical profiles of concentration of transparent exopolymeric particles (TEP) and Coomassie stainable particles (CSP) in GB (C) and LD (F) Grey lines as figure 2.

Figure 4. Vertical profiles of MnOx-like particles and O₂ concentration in the water column at the location of the sediment traps deployments. (A) GB and (B) LD. Grey lines as in figure 3.

Figure 5. Vertical fluxes of particulate organic carbon (POC) and particulate nitrogen (PN) as well as oxygen concentration in GB (A) and LD (C). Vertical fluxes of particulate organic phosphorus (POP), biogenic silica (BSi) and chlorophyll *a* (Chl *a*) in GB (B) and LD (D).

Figure 6. TEP and CSP fluxes in GB (A and B) and LD (C and D). In addition to vertical fluxes, each profile is complemented with microscopic images (200x) of material collected at each depth. In GB, star-shaped MnOx-like particles are clearly visible as single particles and forming aggregates with TEP (A), and CSP (B). MnOx-like particles were less abundant in LD (C and D). (F) A larger magnification (400x) image of MnOx-like particles at 110 m showing more detail on the shape of those particles and aggregates formed with TEP.

Figure 7. Vertical fluxes of total hydrolyzable amino acids (TAA) and total carbohydrates (TCHO) as well as oxygen concentration in (A) GB, and (B) LD.

Table 1. Sediment traps deployment and recovery locations, dates, collection times and depths. Two sediment traps were deployed at 40 m (A and B) to evaluate replicability.

Station	Lat	Lon	Date	Station depth	Deployment time (d)	Trap depths (m)
Gotland Basin (GB)	57.21 °N	20.03 °E	08/06/2015	248 m	2	40A, 40B, 60, 110, and 180m
	57.27 °N	20.25 °E	10/06/2015			
Landsort Deep (LD)	58.69 °N	18.55 °E	15/06/2015	460 m	1	40A, 40B, 55, 110, and 180m
	58.68 °N	18.68 °E	16/06/2015			

Table 2. Abundance of chlorophyll and phycoerythrin containing pico- and nano-plankton measured by flow cytometry in GB and LD.

	Depth (m)	Phytoplankton (cells mL ⁻¹)			Cyanobacteria-like (cells mL ⁻¹)		
		picoplankton	nanoplankton	Total	picoplankton	nanoplankton	Total
GB	1	87963	2097	90060	5225	731	5956
	10	94369	2628	96997	8795	920	9716
	40	4999	68	5067	2174	69	2243
	60	4125	35	4160	1990	42	2032
	80	599	7	606	238	15	253
	110	594	7	601	326	29	356
	140	1144	14	1158	356	2	358
	180	908	9	917	366	20	385
	220	2270	19	2289	1063	34	1097
LD	1	92359	2283	94642	834	177	1011
	10	86426	1708	88134	2990	232	3223
	40	2022	92	2114	2243	69	2312
	60	1524	62	1586	1294	24	1318
	70	908	43	951	613	17	630
	110	1735	82	1817	1181	17	1198
	180	1339	75	1415	946	34	980
	250	1593	82	1676	949	36	985
	300	1521	48	1569	1047	17	1064
	350	1608	57	1665	908	12	920
	400	1548	73	1621	1047	22	1069
	430	1562	68	1631	875	19	894

Table 3. Phytoplankton abundance analyzed microscopically for samples collected at the location of trap deployment in GB and LD.

		Phytoplankton Abundance (L ⁻¹)							
		GB				LD			
		1 m	10 m	40 m	Total	1 m	10 m	40 m	Total
Cyanobacteria*	Total	14148	13536	0	27684	37368	32526	96	69990
Chryptophyta	Total	140	112	28	280	1400	882	56	2338
Bacillariophyceae	Total	96	94	44	234	462	112	102	676
	<i>Chaetoceros</i> sp.	58	42	24	124	434	106	26	566
	<i>Skeletonema</i> sp.	26	8	12	46	12	0	8	20
	<i>Thalassiosira</i> sp.	12	44	8	64	16	6	68	90
Dinophyceae**	Total	3772	4424	1192	9388	9032	7662	1404	18098
	<i>Dinophysis</i> sp.	678	742	2	1422	450	214	4	668
	other	3094	3682	1190	7966	8582	7448	1400	17430
Chlorophyta	Total	5320	6860	28	12208	2072	1022	238	3332
	<i>Planctonema</i> sp.	5320	6860	28	12208	2072	1022	238	3332

*Filamentous cyanobacteria were counted in 50 µm length units (>90% were *Aphanizomenon* sp.)

**Include mixotrophs

Table 4. MnOx-like particle fluxes and size as equivalent spherical diameter (ESD) determined by image analysis in GB and LD.

Station	Depth (m)	MnOx-like particles ($\text{cm}^2 \text{m}^{-2} \text{d}^{-1}$)	Median size ESD (μm)	Size range ESD (μm)
GB	110	5666 \pm 994	2.8	0.6-167
	180	7789 \pm 955	3.3	0.6-153
LD	110	50.3 \pm 1.8	1.8	0.6-16.5
	180	2.6 \pm 0.3	1.4	1.2-9.3

Table 5. Amino acids (AA), carbohydrates (CHO), elemental molar ratios and amino acid-based degradation index of sinking and suspended particles in GB and in LD.

		Depth (m)	AA-C:POC %	CHO-C:POC %	POC:PN	POC:POP	POC:BSi	PN:BSi	PN:POP	DI
Sinking particles	GB	40	19.2	18.3	9.8	244	3.9	0.4	24.9	1.49
		40	17.6	17.2	9.4	222	4.1	0.4	23.6	1.43
		60	15.8	17.6	9.5	232	2.8	0.3	24.3	1.13
		110	13.9	22.2	11.3	90.1	1.7	0.2	8.0	0.71
		180	11.1	18.5	12.7	123	3.0	0.2	9.7	-0.03
	LD	40	13.5	9.4	12.2	772	3.6	0.3	63.4	0.30
		40	14.3	8.4	11.1	413	4.1	0.4	37.2	0.27
		55	19.1	11.0	12.4	332	3.0	0.2	26.7	-0.02
		110	13.4	12.0	15.4	230	2.7	0.2	14.9	0.11
		180	14.3	12.9	15.3	341	4.2	0.3	22.3	-0.29
Suspended particles	GB	1	8.2	16.9	10.4	155	91.4	8.8	14.9	
		10	10.8	8.8	10.5	151	87.1	8.3	14.4	
		40	4.9	2.8	9.2	88.8	134	15	9.7	-0.81
		60	5.4	2.7	9.8	127	125	13	13.0	-0.27
		80	4.7	0.00	10.4	145			13.9	
		110	9.0	6.6	8.5	245			29.0	0.98
		140	5.3	0.00	10.6	283			26.7	
		180	5.7	4.3	11.4	506			44.5	-0.40
	220	8.6	3.3	12.1	271			22.5		
	LD	1	7.0	0.00	8.7	205	515	59.5	23.7	
		10	13.0	9.1	8.4	196	101	12.0	23.3	
		40	0.00	8.9	8.1	336	24.5	3.0	41.5	-0.53
		60	6.1	10.3	7.8	301	16.9	2.2	38.4	-0.12
		70	7.9	10.7	7.7	292	248	32.1	37.9	
110		12.2	5.4	7.9	225			28.3	0.80	

180	10.1	11.3	7.0	205	29.2	0.34
250	12.0	8.8	6.5	249	38.2	
300	10.9	0.00	6.7	137	20.4	
350	10.7	10.1	6.8	146	21.6	
400	10.0	0.00	6.2	230	37.2	
430	9.4	9.5	7.8	149	19.0	

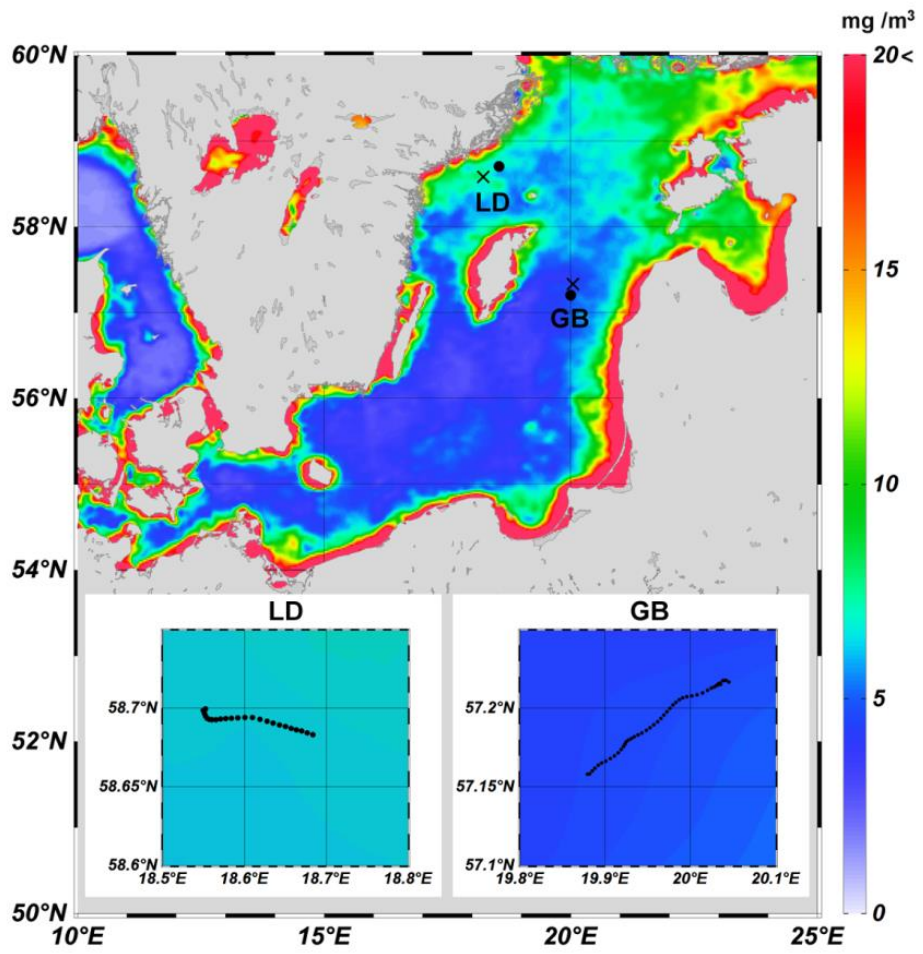


Fig. 1

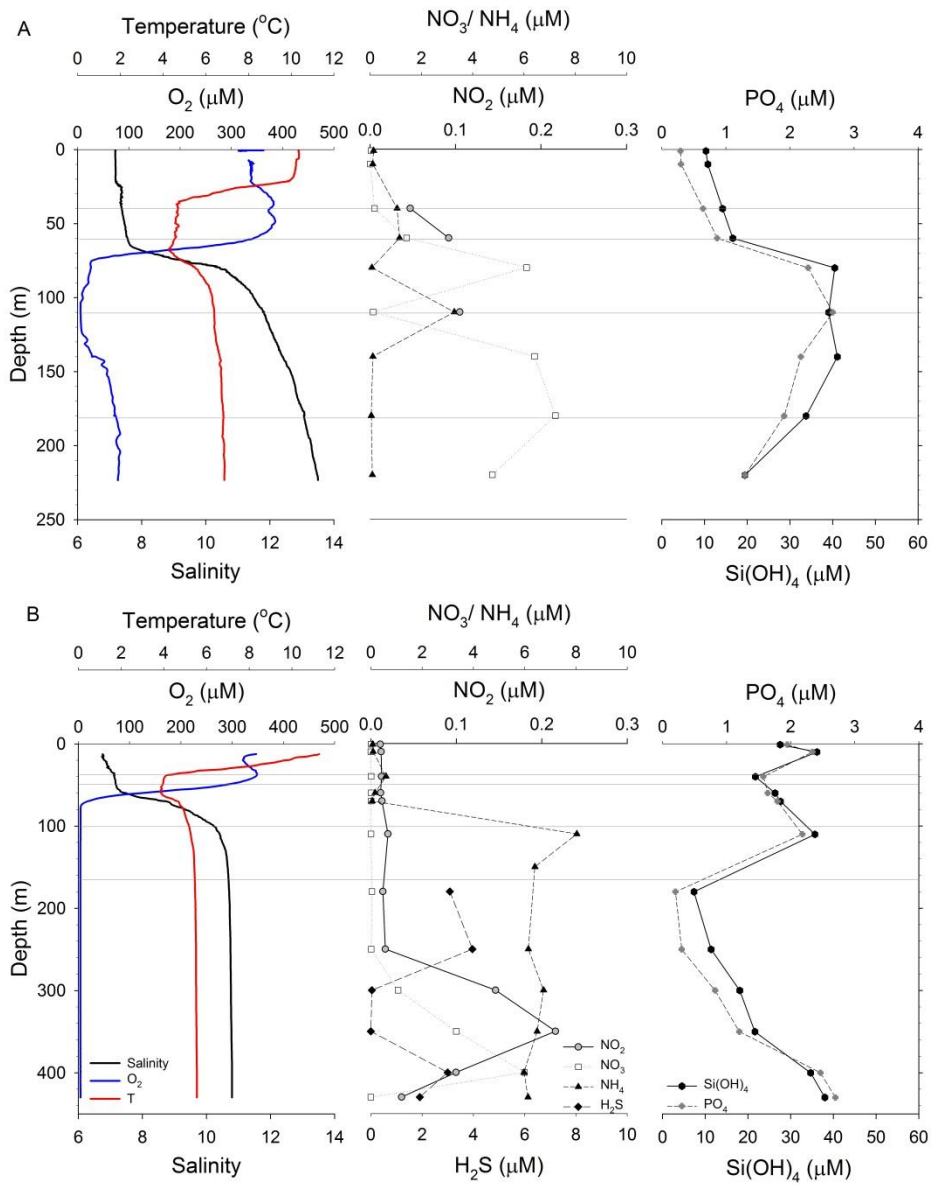


Fig. 2

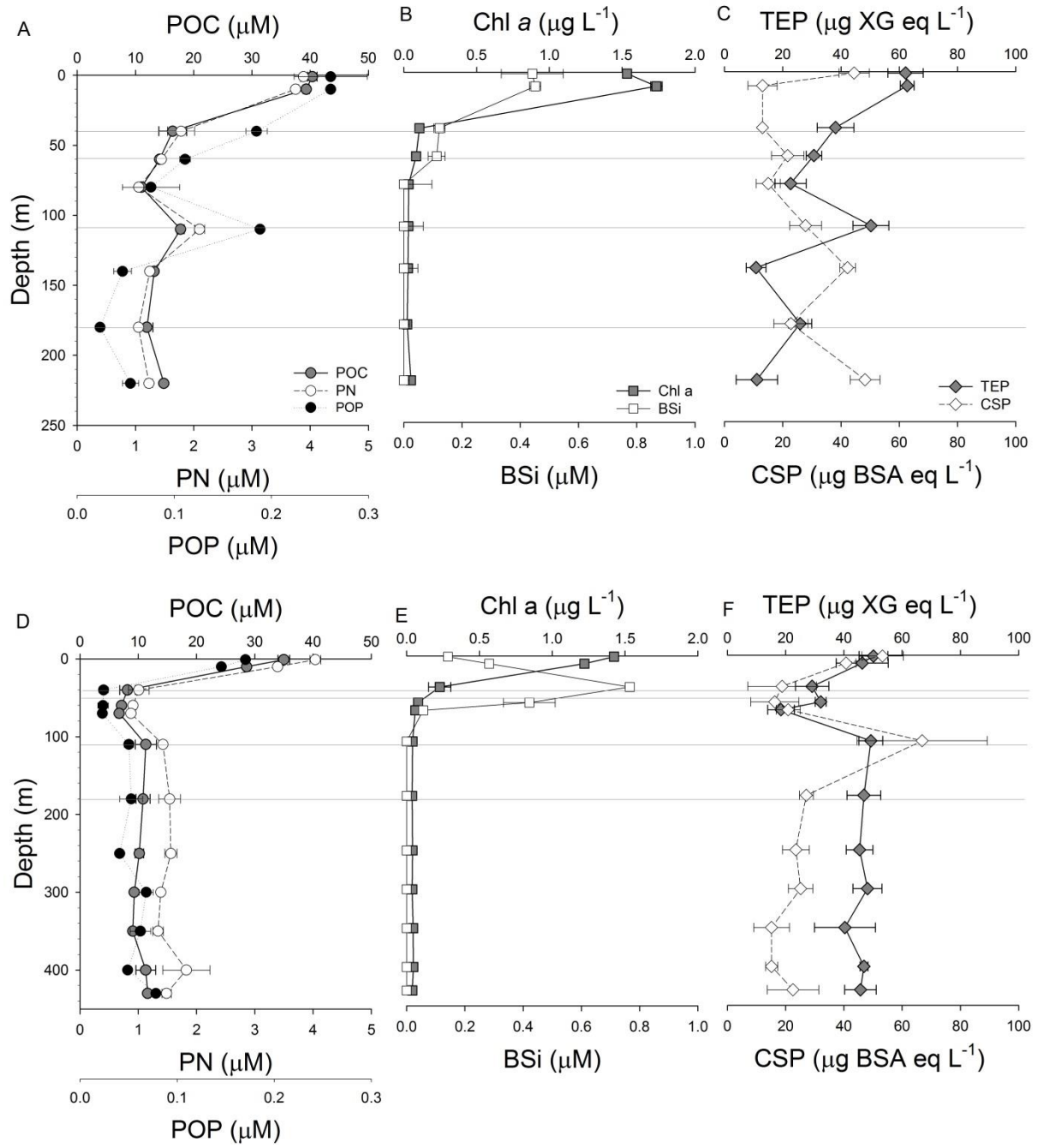


Fig. 3

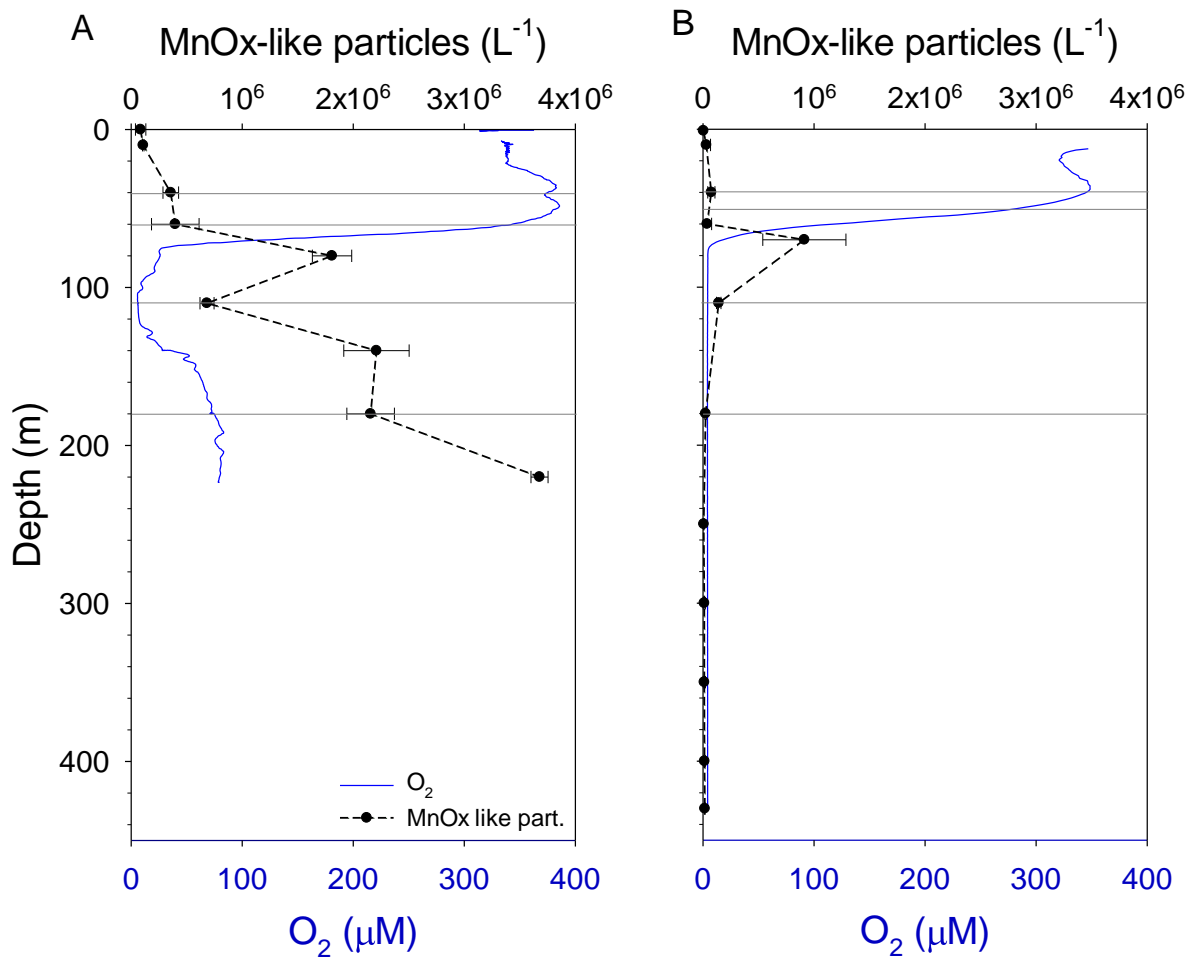


Fig. 4

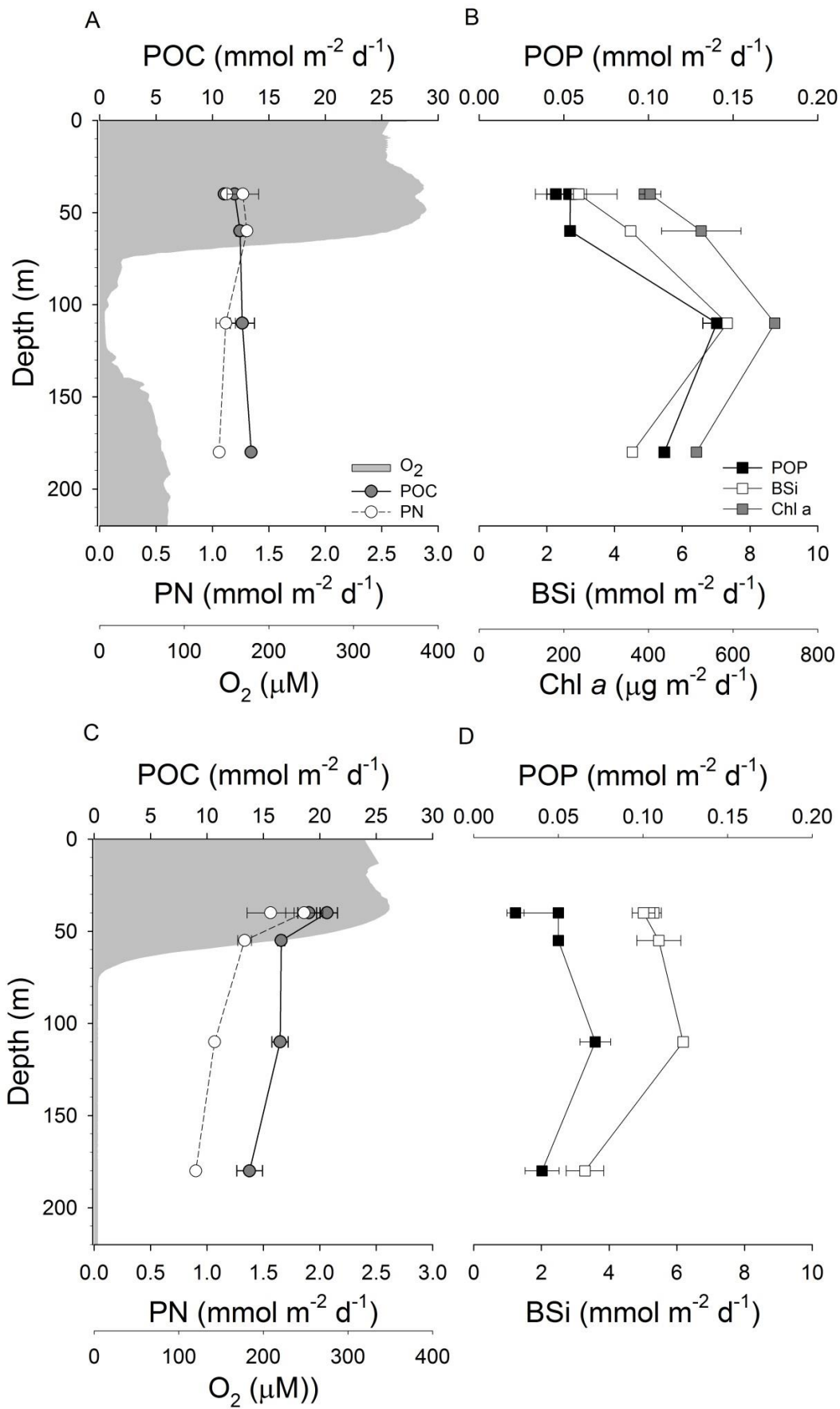


Fig. 5

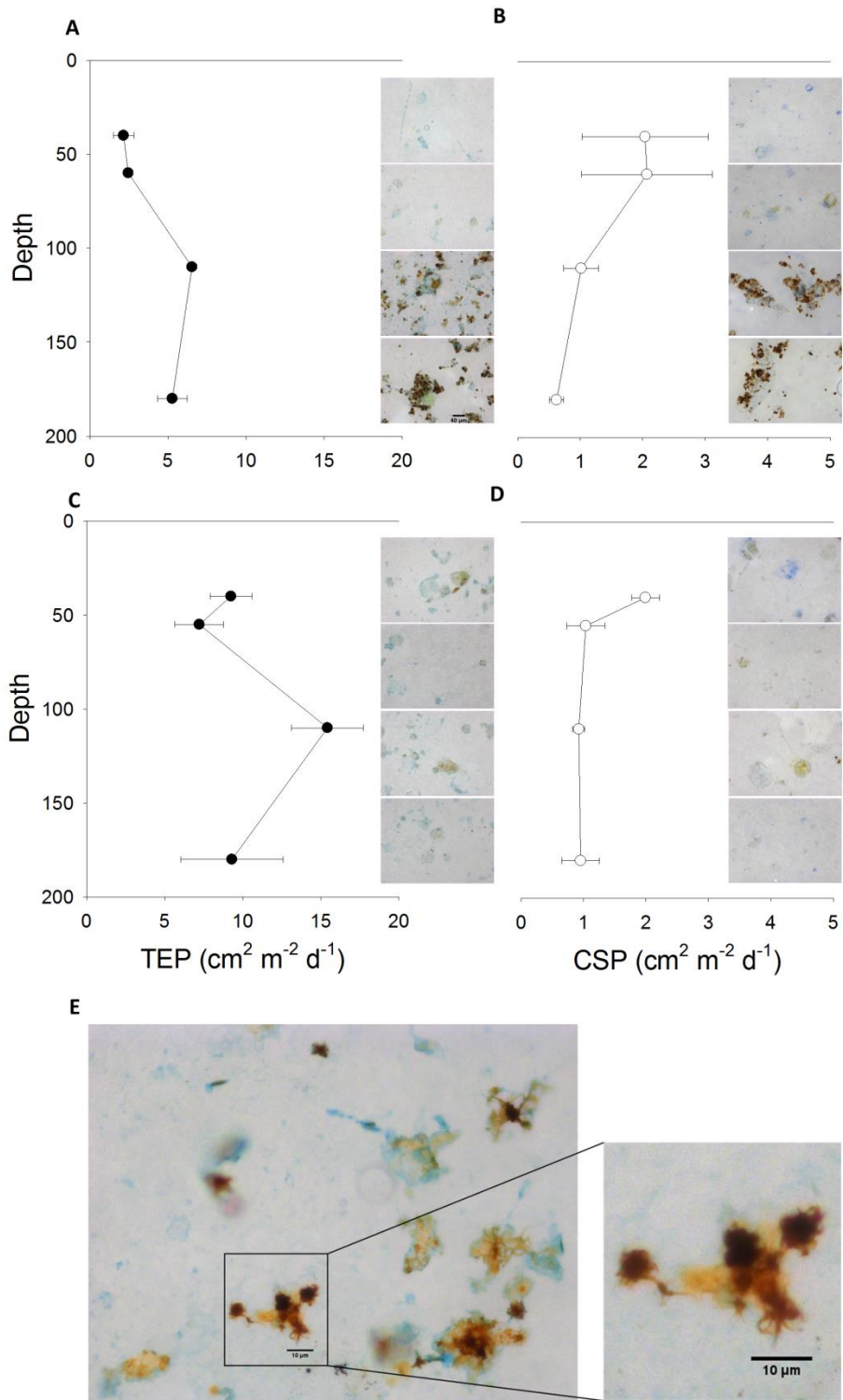


Fig. 6

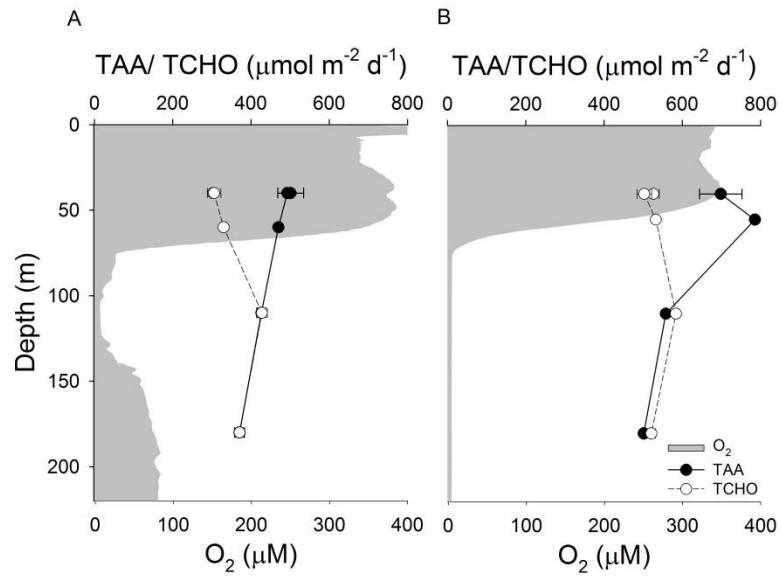


Fig. 7